AGU **ADVANCING EARTH AND SPACE SCIENCE**

JGR Solid Earth

Key Points:
- New paleointensity results using the multispecimen parallel differential partial thermoremanent magnetization (pTRM) method with domain-state corrections
- Comparison and combination of multispecimen and Thellier-type paleointensity methods applying and analyzing different selection criteria
- High-quality low Pliocene paleointensities obtained with a multimethod approach

Supporting Information:
Supporting Information may be found in the online version of this article.

Correspondence to:
E. M. Sánchez-Moreno,
emmoreno@fc.ul.pt

Paleointensity Results From Pliocene Lavas of the Lesser Caucasus Obtained Using the Multispecimen Parallel Differential pTRM Method: A Comparison With Thellier-Thellier and IZZI Data

Elisa M. Sánchez-Moreno[1,2] , Manuel Calvo-Rathert[2] , Avto Goguitchaichvili[3], George T. Vashakidze[4] , Pierre Camps[5] , Juan Morales-Contreras[3] , Néstor Vegas-Tubía[6], and Vladimir A. Lebedev[7]

[1]Instituto Dom Luiz (IDL), Faculdade de Ciências, Universidade de Lisbon, Lisbon, Portugal, [2]Departamento de Física, EPS Campus Rio Vena, Universidad de Burgos, Burgos, Spain, [3]Laboratorio Interinstitucional de Magnetismo Natural, Instituto de Geofísica Unidad Michoacán, UNAM – Campus Morelia, Morelia, México, [4]Alexandre Janelidze Institute of Geology, Ivane Javakhishvili Tbilisi State University, Tbilisi, Georgia, [5]Géosciences Montpellier, Université de Montpellier, CNRS, Montpellier, France, [6]Departamento de Geodinámica, Universidad del País Vasco UPV/EHU, Leioa, Bizkaia, Spain, [7]Institute of Geology of Ore Deposits, Petrography, Mineralogy and Geochemistry – Russian Academy of Sciences (IGEM RAS), Moscow, Russia

Abstract We report paleointensity results obtained with the multispecimen method (MSP) over the Pliocene sequence of Apnia (Georgia) which records a polarity reversal. Paleointensity determinations with the multispecimen technique were performed on 12 flows with the original (MSP-DB) and the domain-state corrected (MSP-DSC) protocol. Eight MSP-DSC determinations passed the proposed quality criteria. To obtain highly reliable data through the agreement between intensity values from different methods, MSP results were combined with paleointensities from a previous study with Thellier-type methods and especially strict selection criteria (RCRIT) on same flows (Sánchez-Moreno et al., 2020). Application of this multimethod procedure resulted in three new paleointensities including both MSP and Thellier-type results and an additional one obtained with two different Thellier-type methods, yielding one paleointensity of 36.9 µT in the normal-polarity, and three paleointensities between 19.2 and 24.1 µT in the reverse-polarity section. Additionally, Thellier-type data have been reinterpreted in this study with more flexible criteria (TTP) and the results combined with the MSP data. As a result, four flows yield paleointensities including MSP and Thellier-type determinations and seven include paleointensities obtained with two different Thellier-type methods. Results range from 37.2 and 44.3 µT in the normal-polarity and from 12.5 to 24.6 µT in the reverse-polarity section. Comparison of results from the four flows yielding multimethod determinations applying RCRIT criteria with those from the same flows under TTP criteria yields no significant difference in paleointensity values and their experimental uncertainty. Thus, application of a multimethod approach supports the possibility of using TTP criteria.

1. Introduction

Both directional and intensity data are crucial to deeply understand the features of the Earth's Magnetic Field (EMF) during unstable periods such as reversals or excursions. Nevertheless, the number of paleo-intensity references available in the databases is much lower than the directional ones due to the require-ments and difficulties related to its determination. Furthermore, obtaining paleointensity data representing the true field strength is conditioned by the response of the different determination methods and the selec-tion criteria applied.

Whereas paleomagnetic directions are normally parallel to the field direction and therefore able to provide direct information about the EMF, the determination of the absolute paleointensity involves more compli-cated protocols and is more time-consuming. This difficulty is owed to the fact that the remanent magnet-ization and the EMF are different physical quantities and their magnitudes are not equal but proportional (in the case of weak fields). Moreover, there are processes that can alter the constant of proportionality that links both quantities. A further conditioning factor for absolute paleointensity determinations is the

reproducibility of the magnetization acquisition at the laboratory. Therefore, it is only possible to recover the ancient field from materials that have undergone heating and present a thermoremanent magnetization (TRM), such as volcanic rocks and archeological pieces.

During paleointensity experiments, it must be considered that the multiple heating and cooling steps may result in magneto-chemical alteration of the carriers of remanence. Moreover, samples need to obey the Thellier laws of reciprocity, independence, and additivity of partial thermoremanent magnetization (pTRM). This is only the case of the TRM recorded by single domain (SD) grains (Dunlop, 2011; Thellier and Thellier, 1959 and references therein), where the blocking and unblocking temperatures of the magnetization are equal. Multidomain (MD) grains (s.l.), on the other hand, are characterized by different blocking and unblocking temperatures giving rise to so-called pTRM tails (Bol'shakov and Shcherbakova, 1979; Dunlop and Xu, 1994), which "add" an extra magnetization to the original one, recorded during the cooling of the material studied. The methods of paleointensity determination and the success of the results will depend on the proportion of the different grain sizes.

The present study jointly analyzes new absolute paleointensity data obtained through the multispecimen method (MSP; Biggin & Poidras, 2006; Dekkers & Böhnel, 2006; Fabian & Leonhardt, 2010) and a collection of Thellier-type paleointensity determinations performed previously (Sánchez-Moreno et al., 2020) with the Thellier-Thellier (TT; Thellier and Thellier, 1959) and the IZZI (Yu et al., 2004) methods, interpreted under a strict selection criteria set (RCRIT) based on Tauxe et al. (2016). Paleointensity determination methods depend on how different energy equilibrium states are reached during the experiments. These equilibrium states vary according to different factors such as temperature, applied field or demagnetizing field. Therefore, the use of different methods relying on different experimental processes on samples of the same units, provides a supplementary strong reliability proof by means of a multi-method consistency check (Biggin & Paterson, 2014; Biggin et al., 2015; Calvo-Rathert et al., 2016; De Groot et al., 2013, 2015, 2016; Monster, de Groot, Biggins, Dekkers , 2015; Monster et al., 2018). The special interest of a multi-method approach derives from the need to obtain high reliability intensity data. When we analyze the global intensity database, we can see disagreements between data from similar locations and ages and a wide bias in the geographic distribution. Reliable data are necessary to understand how the intensity behaves during and near polarity changes, as well as during stable periods. The time-averaged value of the EMF strength is the topic of an ongoing intense discussion (e.g., Goguitchaichvili et al., 1999; Heller et al., 2002; Juarez & Tauxe, 2000; Lawrence et al., 2009; McFadden & McElhinny, 1982; Tanaka et al., 1995; Tauxe et al., 2013; Valet & Fournier, 2016; Valet et al., 2005; Wang et al., 2015). Moreover, this work provides an interesting study of the sample behavior with mixtures of single domain (SD) and multidomain (MD) grains under different methodologies, one of them (MSP) applicable to remanences carried by MD-grains.

The multispecimen parallel differential pTRM method (MSP-DB; Biggin & Poidras, 2006; Dekkers & Böhnel, 2006) is a relatively new paleointensity method, which presumably does not depend on magnetic domain structure because it likely eliminates the effect of magnetic history. The protocol proposes to perform a single heating, trying to minimize the effect of magnetic history due to the presence of MD grains. Fabian and Leonhardt (2010), however, suggest that even so, this method systematically overestimates paleointensity and propose some additional steps to pTRM normalization, domain-state correction and alteration test in a new protocol named multispecimen domain-state-correction (MSP-DSC). Paleointensity overestimates have also been observed by Michalk et al. (2010, 2008) and Calvo-Rathert et al. (2016) using the MSP-DB method on volcanic rocks with a considerable MD fraction.

In the Thellier-type determinations performed by Sánchez-Moreno et al. (2020) on the Apnia sequence, the selection criteria RCRIT applied were especially strict, yielding results in 8 lava flows of the 20 that make up the sequence. However, some set of criteria can be too strict, as they lead to the rejection of ideal samples subject to experimental noise (Paterson et al., 2014a). In other words, the low quality of some samples, represented by the values of the selection criteria, may be caused by problems during experimental measurements and not by the magnetic characteristics of the sample itself. Taking this perspective, in the present study the reinterpretation of previous Thellier-type data has been performed using a set of less strict criteria based on the common ThellierTool criteria set (Leonhardt et al., 2004) modified by Paterson et al. (2014a, 2014b), named here TTP.

The main goal expected to be achieved by the combined analysis of MSP and Thellier-type data, the latter under two selection criteria sets of different strictness, is gathering highly reliable paleointensities by combining the results from several methods. This leads us to reach two more objectives:

- Obtaining new paleointensity data in the Apnia sequence by applying a different method: The multispecimen parallel differential pTRM method (Biggin & Poidras, 2006; Dekkers & Böhnel, 2006) with domain-state corrections (Fabian & Leonhardt, 2010).
- Use of these new data to study the effect of data selection on paleointensity results by comparing: (1) MSP with Thellier-type results and (2) the Thellier-type results applying two selection criteria sets with different degrees of strictness.

As a result of this data analysis, the new multi-method results are used in the interpretation of the paleointensity variation through the basaltic lava flow sequence of Apnia (Djavakheti Highland, Southern Georgia). The paleomagnetic directions obtained in this sequence, display either a reversed to normal geomagnetic polarity transition record (Figure S1 and S3), likely the Gilbert-Gauss reversal, or a combined transition register including chron C2Ar to subchron C2An-2n (Sánchez-Moreno et al., 2018).

2. Geological Setting

The studied lava flow sequence (41° 21′ 57.4" N, 43° 16′ 21.8" E) is located near the village of Apnia in the volcanic Djavakheti Highland region. This volcanic region lies in the central sector of the Lesser Caucasus in Southern Georgia (Figure S1.). The Lesser Caucasus belongs to the Alpine-Himalayan belt and is being generated by the still active collision of the Arabian and Eurasian plates. In the Lesser Caucasus area, different phases of volcanic activity have taken place (Lebedev et al., 2008) during the so-called post-collision stage (Adamia et al., 2011). The volcanism that generates the lavas analyzed in the present study corresponds to the 3.7–1.8 Ma phase. This phase is characterized by specific features like numerous volcanic cones and fissure volcanoes generated by NW-SE and NE-SW extensional strike-slip structures, which resulted from the compressional regime (Avagyan et al., 2010). This volcanism shapes the Djhavakheti and Armenian plateaus and has been named Akhalkalaki formation in the Djhavakheti region (Maisuradze & Kuloshvili, 1999).

Twenty consecutive lava flows of tholeiitic basalt composition make up the Apnia sequence (Figure 1). Sampling was performed from top (AP01) to base (AP19) and between 6 and 12 cores were taken from each successive flow using a transportable water-cooled drill. Some flows were not sampled in stratigraphic order, so in Figure 1 (and in the tables shown in this publication), the numbering is not consecutive in some cases (e.g., AP02, AP04, AP05, AP03). They were oriented directly in the field by means of a magnetic and a solar compass as well as an inclinometer.

The lowermost dated flow yields a K-Ar age ($\pm 2\sigma$) of 3.70 ± 0.20 Ma (flow AP11) and the uppermost one 3.09 ± 0.10 Ma (flow AP01; Lebedev et al., 2008). In addition, two more dates in flows AP05 and AP08 provide ages of 3.28 ± 0.10 Ma and 3.75 ± 0.25 Ma respectively (Lebedev et al., 2008).

3. Preceding Paleomagnetic and Rock Magnetic Studies

The analysis of paleomagnetic directions obtained from the Apnia volcanic sequence is consistent with a record of a polarity reversal having taken place between 3 and 4 Ma (Sánchez-Moreno et al., 2018). A succession of 14 lava flows of reversed polarity is shown in the lower part, whose average pole differs from the expected one (Figure S3). The reversed polarity flows are overlain by a single flow showing an intermediate virtual geomagnetic pole (VGP) latitude of 12.5° and therefore considered to have recorded a transitional field. On the top, five lava flows display normal polarity, with a mean pole further away from the expected pole than the mean pole of the underlying reverse polarity section. However, the possibility that this discrepancy is due to tectonic rotations has been ruled out (Sánchez-Moreno et al., 2018). Therefore, to explain the directional data of the Apnia sequence, the following interpretations have been put forward: A short emplacement time preventing PSV averaging and/or an anomalous EMF record. In the second case, the Apnia sequence records the Gilbert-Gauss polarity reversal or a combined transition from chron C2Ar to subchron C2An-2n.
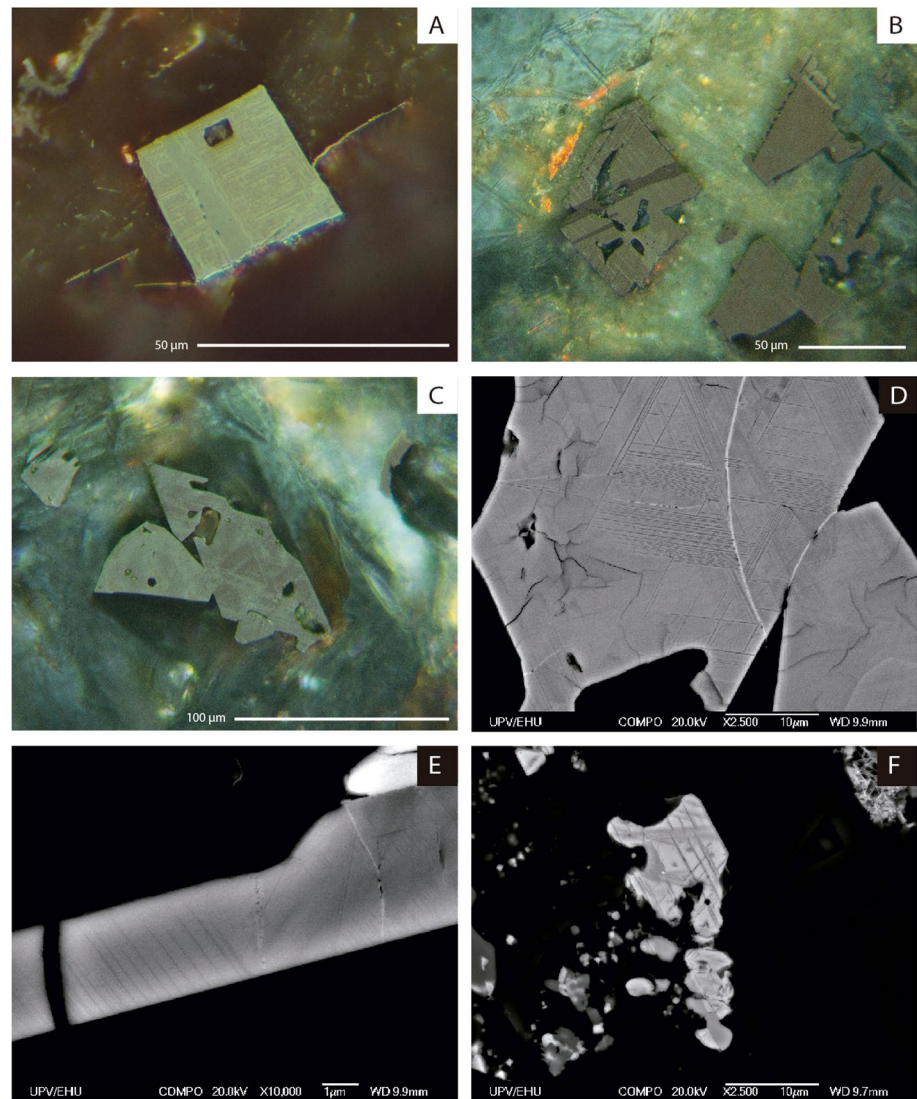
Figure 1. Reflected light optical microscope (a, b and c) and scanning electron microscope (SEM) (d, e and f) images of polished thin sections from the Apnia sequence. (a) and (b) Euhedral titanomagnetite crystal from AP13 with Trellis and Sandwich intergrowths of ilmenite, indicative of a C3 oxidation stage. (c) Titanomagnetite crystal with Trellis ilmenite intergrowths pointing out a C3 oxidation stage (AP06). (d) Detailed image of a titanomagnetite crystal from AP06 with Trellis intergrowths of ilmenite, indicative of C3 oxidation stage, and micro-cracks around the crystal boundaries due to maghemitization. (e) Detail of an acicular ilmenite crystal showing exsolved rutile needles, evidence of R2 oxidation stage. Sample AP06. (f) Titanomagnetite crystal with Trellis and Sandwich ilmenite intergrowths pointing out a C3 oxidation stage (AP08).

A comprehensive set of rock-magnetic experiments was carried out by Sánchez-Moreno et al. (2018) which included IRM acquisition and backfield curves, hysteresis loops and strong field magnetization versus temperature (Ms-T) curves (Figure S4 and S5). The Ms-T curves have made it possible to detect samples with irreversible thermomagnetic behavior, which have not been selected for the paleointensity determinations. The Ms-T curves also show titanomagnetite with different titanium content as the main carrier of magnetization. Hysteresis ratios plot in the "PSD" box of the Day-plot (Day et al. (1977) modified by Dunlop (2002)), which can be explained by a mixture of single domain (SD) and multidomain (MD) or the presence of grains with a transitional state between both states, a so-called vortex state (Roberts et al., 2018). As might be expected, natural samples can include all three states. The presence of MD grains allows us to expect reliable paleointensities when applying the MSP method. MSP is based on the fact that the de-magnetization and remagnetization processes of pTRMs produce certain effects in the TRM of MD grains

with first-order symmetry, similar to those produced in the TRM of SD grains, when they are not subjected to high stress (numerous heating; Biggin & Poidras, 2006). In addition, the corrections added by Fabian and Leonhardt (2010), allow to detect effects caused by differences between demagnetized and overprinted pTRMs in MD grains.

4. Methods

4.1. Reflected Light Optical Microscope and Scanning Electron Microscope

Polished thin sections have been analyzed with reflected light optical microscope and scanning electron microscope (SEM) to check the thermoremanent origin of the magnetization, as well as to characterize with more precision, the nature of the mineral carriers of remanence, regarding the textures, morphologies, distribution, and sizes of the opaque minerals (i.e., mainly titanomagnetites, see section 2).

Based on the different behaviors of the Ms-T curves (Figure S4), five samples from the Apnia sequence were selected, two belonging to type H and one to of each of the three remaining types H*, M, and L. The reflected light optical microscopy was carried out in Géosciences Montpellier (Université de Montpellier, France) with a Leitz Orthoplan Microscope. Elaboration of the polished thin sections, backscattered images and composition analyzes were obtained at Universidad del País Vasco (UPV/EHU, Bilbao, Spain). The polished thin sections were carbon coated and analyzed with a JEOL JSM-7000F SEM equipped with an Oxford Inca Pentafet X3 energy dispersive X-ray analyzer (EDX). The EDX microanalyzes were performed with a backscattered electron signal (BSE) at 20 kV and a current intensity of 1×10^{-19} A, with a working distance of 10 mm.

4.2. Multispecimen Protocol

The multispecimen parallel differential pTRM method (MSP-DB; Biggin & Poidras, 2006; Dekkers & Böhnel, 2006) was proposed as a technique fitted to estimating paleointensities independently of domain states of magnetic minerals. Different fields (B_{lab}) are applied to several sister specimens of each sample, parallel to the original TRM and at the same temperature (Table S1). The temperature is chosen to avoid magneto-chemical transformations, but it must be sufficient to create a pTRM spanning an adequate fraction for the paleointensity determination. Therefore, the method provides two advantages over the Thellier type methods: (1) The magnetic history effects are eliminated and (2) the number of heatings is drastically reduced and the temperature applied is selected to avoid magneto-chemical alterations. Correction steps have been introduced in order to prevent the possible paleointensity overestimation observed in some previous studies (Calvo-Rathert et al., 2016; Fabian & Leonhardt, 2007; Michalk et al., 2008, 2010), questioning the theoretical model first introduced by Biggin and Poidras (2006). The complete MSP-DSC (Fabian & Leonhardt, 2010) adds three additional heating-cooling cycles (Table S1). The new steps allow for the correction of the TRM fraction involved in the determination (MSP-FC), reducing the pTRM-tail effect from MD grains (MSP-DSC), and the calculation of the relative alteration produced (ε_{alt} in Tables 1 and S1.).

Measurements were carried out in two different laboratories: Servicio Arqueomagnético Nacional Universidad Nacional Autónoma de México (UNAM), Morelia (México) and Géosciences, Université de Montpellier (France). The online version Multispecimen Paleointensity 1.5. software (http://ambre.gm.univ-montp2.fr/camps/MSP_DSC/) has been used for the interpretation of MSP results.

The sample pre-selection criteria in the UNAM laboratory were the following: a univectorial ChRM component, the presence of reversible Ms-T curves (type H and H* in Sanchez-Moreno et al. (2018) and Figure S4), a median destructive field (MDF) > 25 μT in alternating field (AF) demagnetizations and magnetization drops at high temperatures in the thermal demagnetization experiments. The chosen temperature was 450°C, where at least 25% of the initial natural remanent magnetization (NRM) is lost in the thermal demagnetization. Therefore, we try to ensure that at least 20% of NRM is involved in the experiment, while the temperature is low enough to avoid magneto-chemical alteration in the selected samples. We had to select the same temperature for several samples at the same time, since the field was applied to groups of seven specimens from different samples, due to the type of furnace and sample holder used in it.

Table 1
Selection Criteria of the Multispecimen Paleointensity Determinations

Criteria thresholds applied to each specimen-B_{lab} point results			
Cook's D	$\leq$	3 cook's D mean	Cook's Distance: Influence of each specimen-B_{lab} point in the OLS or WLS regressions. It is a default software requirement to evaluate the measure quality in MultiSpecimen Paleointensity software online version (http://ambre.gm.univ-montp2.fr/camps/MSP_DSC/).
f	=	0.2–0.8	Ratio between NRM fraction removed and overprinted by the laboratory pTRM for each specimen-B_{lab} point (Fabian & Leonhardt, 2010). It is obtained from the half vector sum between m1 and m2 normalized by the NRM, so that it is only calculated for FC and DSC. Even so, it is also applicable to DB. f depends on the temperature reached, which is the same in the three MSP variants. It ensures that, if present, the multidomain pTRM tail effect (Dunlop & Özdemir, 2000) is correctly measured. The fraction of unblocked NRM during the heatings must be between 20% and 80% of the total NRM, as in that interval, because it is large enough to be accurately measured and it is below the total TRM (Carvallo et al., 2017; Tema et al., 2016).
Crit-angle	$\leq$	10°	Critical angle: Maximum angle between the NRM remaining after the pTRM acquisition and the total NRM. This criterion ensures that the NRM is the ChRM (Tema et al., 2016).
m4m3 m1m3		m4 > m3 m1 > m3	Intensity difference between m4−m3 and m1−m3 steps. It is used as an alteration test. It is a default software requirement to evaluate the measure quality in MultiSpecimen Paleointensity software online version (http://ambre.gm.univ-montp2.fr/camps/MSP_DSC/).

Criteria applied to complete paleointensity determination			
Class		A	B	Determination quality level.
n	$\geq$	4	3	Number of specimen-B_{lab} points taken in the determination. The relation N/n also must be taken into account since results comparison. N = total number of specimen-B_{lab} points.
f-range	=	0.3–0.7	0.2–0.8	Minimum and maximum ratio between the fraction of NRM removed and overprinted by the laboratory pTRM of the total specimens-B_{lab} points used in the paleointensity calculation. It allows to evaluate the NRM fraction removed and overprinted in the complete determination.
$CI_{95\ T/2}$ (%)	$\leq$	25	25	95% confidence interval of the determination, divided by two. It is calculated through bootstrapped of 500 values with the MultiSpecimen Paleointensity software online version (http://ambre.gm.univ-montp2.fr/camps/MSP_DSC/). It is really only valid if the bootstrapped values have a Gaussian distribution. It is a perfect determination when the upper and lower limits are symmetrical with respect to the paleointensity value. The parameter is less reliable, than fewer points the determination includes. Is taken as similar to the σB error in single Thellier-type determinations to make them comparable.
R_2	$\geq$	0.9	0.85	Quality of the OLS or WLS regressions fit. It evaluates the lineal dependence between Blab and Q ratios.
ε_{alt} (%)	$\leq$	10	20	Relative alteration error average % (Fabian & Leonhardt, 2010). When thermo-chemical changes occur, the temperature attained is more important than the number heatings, hence it is possible to use ε_{alt} for the all MSP protocols. Value A taken from Tema et al. (2016) and B from Carvallo et al. (2017). $$\varepsilon alt = \left| \frac{m_1 - m_4}{m_1} \right|$$

Table 1
Continued

ΔB (%)	≤	20	25	Final error obtained from alteration error plus domain-state-correction error (ΔH in Fabian & Leonhardt, 2010). As with the alteration error, it depends on the temperature reached, so that it can be applied to MSP-DB, FC and DSC $\left(\dfrac{\Delta H}{H}\right)^2 = \left[\displaystyle\sum_{i=1}^{N}\left(\dfrac{H_i / H}{\Delta Q_i}\right)^2\right]^{-1}$ H: single - specimen paleointensity H_i : laboratory field ΔQ_i : single - specimen total error

Note. OSL, Ordinary Least Squares regression used in MSP-DB and MSP-FC determinations. MSP-DB, multispecimen parallel differential pTRM method; MSP-DSC, multispecimen - domain state correction protocol; MSP-FC, multispecimen - fraction correction protocol; NRM, natural remanent magnetization; pTRM, partial thermoremanent magnetization, WLS, Weighted least Squares regression used in MSP-DSC determinations. Specimen-B_{lab} point: each specimen subjected to a different B_{lab}.

Standard samples were divided into small irregular pieces and fixed in 10 cm³-standard size salt pellets. The salt samples were placed in a mu-metal homemade sample holder, of seven samples capacity, heated with a TD48-DC (ASC) furnace and measured with a JR-6 spinner magnetometer (AGICO).

B_{lab} was applied at intervals of 5 or 10 µT up to 80 µT on seven specimens from each studied lava flow for the MSP-DB protocol and on 4 to 5 specimens for the MSP-DSC protocol. The aim is for the fields applied to be as close as possible to the paleointensity resulting from the determination. Having more data around the expected field would give a more precise determination of the MSP paleointensity values. To restrict this value, first the extreme fields of 5 or 10 and 80 µT were applied to groups of seven specimens from different samples, given that the sample holder, used to apply the oriented field at the samples in the furnace, has a capacity of seven samples for each heating. In the same way, intermediate fields were applied until those closest to the generated paleointensity were found. Sometimes, just one field step to the lower-field side of the paleointensity estimate was applied; unfortunately, this makes the estimate sensitive to changes at the high field steps, which may cause large uncertainties.

In Géosciences – Montpellier, the samples were chosen under the same pre-selection criteria as in UNAM. The heating temperature chosen was also set at 450°C to keep the same conditions as the experiments previously carried out in the UNAM laboratory. B_{lab} was applied in intervals of 10 µT, up to 80 µT, to eight specimens from each selected lava flow. The same field steps were also applied to have the same conditions as at UNAM. Standard samples were broken into small irregular fragments and fixed into 10 cm³-standard size plaster. The samples were heated in the FURéMAG prototype furnace (Patent # 1256194). During heating and/or cooling a precise magnetic induction field, with a precision better than 1°, was applied to each sample. As shown by Fanjat (2012) during the calibration and test of that furnace, it is not necessary to apply a cooling rate correction with the MSP protocol. In addition, vortex/PSD particles show negligible cooling rate dependence, as can be seen, for instance in the experimental study performed by Biggin et al. (2013). Measurements were performed with a superconducting magnetometer (2G Enterprise).

When the samples′ individual declination and inclination measured at different steps were found distinct to the original NRM, they were not corrected, due to the difficulty of calculating the angle of the correct pTRM, due to the effect of pTRM-tails caused by MD grains. However, when the maximum angle between total TRM and the TRM after pTRM acquisition exceeded a critical angle of 10°, the measurement for that specimen was dismissed.

Parameter α (equation 17 in Fabian & Leonhardt, 2010) is a constant to calculate the contribution of the domain state effect, used to avoid a possible overestimate of the domain-state contribution. The value of α is expected to be sample-specific, because it depends on mineralogy, grain size, and heating temperature. In this work, we have calculated the Q_{DSC} ratio with different α values (0.2, 0.5, and 0.8) to evaluate the optimal result. To this end, we will use the correlation coefficient R^2 from the linear regression of the data obtained with each α value.

A set of selection criteria based on the linear regression analysis and correction ratio Q_{DB}, Q_{FC} and Q_{DSC} calculations (Fabian & Leonhardt, 2010) was used to select MSP data rejecting those of poor technical quality. Two sets of thresholds are proposed for these criteria at two levels A and B, where A indicates a very high quality. To see the complete description and thresholds see Table 1. The thresholds from the parameters NRM fraction ratio *f*, critical angle *Crit-angle* and relative alteration error $\mathcal{E}_{alt}$, have been taken from different authors (Carvallo et al., 2017; Fabian & Leonhardt, 2010; Tema et al., 2016) who have tested them experimentally. Moreover, the software used for the interpretation includes some additional requirements like the thresholds of criteria Cook's Distance *Cook's D* and intensity difference between steps m4m3 and m1m3. In this study, it has also been proposed to use certain thresholds for criteria like the number of specimen-B_{lab} points taken in the determination *n*, coefficient of determination R^2, minimum and maximum NRM fraction ratio of the total specimens-B_{lab} points used in the determination *f*-range, 95% confidence interval of the determination divided by two $CI_{95T/2}$ and final paleointensity error ΔB.

Seven MSP determinations on single cores belonging to seven different lava flows were measured in the UNAM laboratory and five were carried out on samples from five different lava flows in Géosciences – Montpellier. In this latter case, the specimens for each determination were taken from a single core in three cases, and from different cores in two cases (cores 03 and 04 separated 40 cm in AP01 and cores 07 and 09 separated 2 m in AP20). MSP paleointensity determinations were carried out on 12 of the 20 flows comprising the Apnia sequence.

4.3. Reinterpretation of Thellier-type Determinations

One of the aims of the present work is to study the effect of data selection on paleointensity results. To this end, the differences between the results obtained with Thellier-Type methods will be analyzed under two sets of selection criteria of different degree of strictness, by comparing them with each other and with the MSP results.

In the previous study performed by Sánchez-Moreno et al. (2020), Thellier-type paleointensity determinations with the IZZI protocol (Yu et al., 2004) and the original Thellier-Thellier (TT) protocol (Thellier and Thellier, 1959) have been carried out on samples from all 20 lava flows of the Apnia sequence. The results were interpreted with an especially strict set of selection criteria (RCRIT) and thresholds (level A and B; Table 2) focused on detecting a high fraction of magnetization used in the determination (FRAC) and a low dispersion of the Arai plot points (SCAT).

However, too strict criteria can cause the rejection of proper results subject to experimental noise (Paterson et al., 2014a, 2014b), as during the performance of the measurements where mistakes can be made in the orientation of the samples, or with problems with temperature and/or field offset of the instruments, etc. For this reason, we have performed a new interpretation over previous Thellier-type determinations (Tables S2 and S3) using a selection criteria set named here TTP (Table 2). These looser criteria set is based on the common ThellierTool criteria (Leonhardt et al., 2004) modified by Paterson et al. (2014a, 2014b) (named TTA and TTB). TTP criteria set include two quality levels, class A and B, where A values indicate high data quality (Table 2). It has a greater emphasis on enhancing the quality of the pTRM checks.

Both sets of criteria, RCRIT and TTP, apply the |k′| parameter to quantify the curvature of Arai plots (Paterson et al., 2011). |k′| is very useful to detect when an Arai plot has two slopes and therefore an important weight of the MD-grains as magnetization carriers.

Table 2
Selection Criteria Sets Applied To The Thellier-Type Determinations

Criteria parameter		TTP		RCRIT	
		(Present work)		(Sánchez-Moreno et al., 2020)	
		A	B	A	B
$n_{measure}$	≥	5	4	4	4
β	≤	0.1	0.15	0.1	0.1
f	≥	0.5	0.35	-	-
FRAC	≥	-	-	0.78	0.6
q	≥	5	2	-	-
SCAT	=	-	-	True	True
GAP-MAX	≥	-	-	0.6	0.6
|k′|	≤	0.164	0.270	0.164	0.300
MAD_{Anc}	≤	7	15	5	12
α	≤	10	15	-	-
DANG	≤	-	-	10	10
δ(CK)	≤	5	9	-	-
n pTRM checks	≥	2	2	2	2
n_{SITE}	≥	-	-	3	3
σB_{SITE} (μT)	≤	3	3	4	6
σB_{SITE} (%)	≤	25	25	10	15

Note. Parameter values of selection criteria for paleointensity determinations in Thellier-Thellier and IZZI experiments to assess the quality of the experiment conditions, the absence of magneto-chemical alterations and the amount of magnetization carried by SD grains. See Standard Paleointensity Definitions v1.1, Patterson et al. (2014b). TTP set of criteria is based on Leonhardt et al., (2014b) modified by Patterson et al. (2014a) (TTA and TTB). RCRIT set of criteria is taken from Tauxe et al., 2016 and applied at same paleointensity determinations in Sánchez-Moreno et al., 2020. Two different strictness levels, class A and class B, have been considered for both sets of selection criteria.

pTRM, partial thermoremanent magnetization.

5. Results

5.1. Polished Thin Sections Analysis

Dominant opaque phases are titanomagnetites and ilmenites with different degrees of intergrowths. Based on the textures, distribution and sizes of the opaque minerals, two groups of samples can be distinguished. One group is characterized by the predominant presence of euhedral to subeuhedral crystals with maximum sizes of 140 µm (samples AP02 and AP06; Figure 1c–1e). In the second one anhedral opaque minerals with skeletal and dendritic growth morphologies are dominant. These crystals show maximum sizes of 75 µm (samples AP08, AP13 and AP14; Figure 1a, 1b and 1f) and correspond to fast cooling sectors of the lava flows.

In the first group, there are homogeneous, non-exsolved, titanomagnetite crystals as well as titanomagnetites with dense ilmenite intergrowths of Trellis and Sandwich types (Figure 1c and 1d). According to Haggerty (1991) these intergrowths correspond to textural stages from C1 to C3 of high temperature (>600°C) oxidation of titanomagnetite. Frequently in basalts, magnetite and ilmenite exsolution is likely produced by oxidation above titanomagnetite T_C during rock formation. This process indicates that an original TRM is most likely recorded. Ilmenite crystals also show evidences of oxidation due to the presence of fine ferrian-rutile needles (Figure 1e) indicative of an oxidation stage R2 (Haggerty, 1991). Moreover, sample AP06 shows several titanomagnetite crystals undergoing maghemitization along the margins (Figure 1d), as a product of low-temperature oxidation (<300°C). This process is related to the low T_C observed in the M_S-T curves (Figure S4d). In the second group, the titanomagnetites show abundant Trellis and Sandwich types of ilmenite intergrowths (Figure 1a, 1b and 1f) categorized as C3 textural stage of oxidation according to Haggerty (1991).

The process of ilmenite intergrowths on titanomagnetites, on the one hand, generates titanomagnetite grains up to 100 times smaller than the original grain, which increases coercivity, but also increases the interaction field, which may complicate paleointensity experiments. On the other hand, the presence of intergrowths allows the verification of a high temperature (above T_C) remanence acquisition, suitable for the type of studies that are carried out in this work. The observed maghemitization is an oxidation process at low temperature produced in later stages when the lava is cooling or is already cold. It indicates a probable secondary magnetization that can blur the direction and the intensity determination. Consequently, the samples where maghemitization is observed are discarded for paleointensity experiments.

5.2. Multispecimen Paleointensities

After applying the proposed criteria thresholds (Table 1) with two different quality levels, class A and B, 5 MSP-DB determinations, from a total of 12 performed, are considered as reliable. Four determinations belong to class B and one to class A (Table 3). The parameters f (NRM fraction ratio), ΔB (paleointensity final error, ΔH from Fabian & Leonhardt, 2010) and ε_{alt} (alteration error) are calculated with the results obtained from the new steps applied in MSP-DSC protocol. However, these parameters may be also taken to MSP-DB, because, in theory, the same processes that generate these errors in MSP-DSC also occur in MSP-DB because the temperature attained is the same. Given this assumption, MSP-DB determinations showing $f < 0.2$ and $\varepsilon_{alt} > 20\%$ in MSP-DSC are considered failed. The determination obtained for flow AP03 shows a high relative error ΔB but meets all other criteria, and hence it has been labeled as class B*.

Seven successful determinations were obtained with the MSP-DSC protocol (Figures 2, 3, S6 and Table 3), three of them belonging to class A (2 with $\alpha = 0.2$ and 1 with $\alpha = 0.8$) and four to class B (3 with $\alpha = 0.2$ and 1 with $\alpha = 0.5$). Sample AP03 again belongs to class B* ($\alpha = 0.2$). MSP-DSC determinations performed in flows AP15 and AP19 do not pass the criteria $f > 0.2$. AP15 also shows a high confidence interval value, while AP19 has a high ΔB (%). AP20 shows a high ΔB (%) and especially the high alteration error ε_{alt} stands out. Even so, the paleointensity values obtained are coherent with those obtained throughout the sequence.

Paleointensities obtained under the MSP-DB protocol range between 13.6 and 67.1 µT, while MSP-DSC paleointensities yield values between 14.2 and 60.9 µT, except for AP05, which despite passing all quality criteria, yields an apparently more anomalous value of 100.4 µT (Table 3).

Table 3
Paleointensity Determinations Obtained With the Multispecimen Methods (Biggin & Poidras, 2006; Dekkers & Böhnel, 2006; Fabian & Leonhardt, 2010)

Site	Spec.	Prot.	N	n	R^2	f-range	B (μT)	CI$_{95}$ (μT)			CI$_{95T/2}$ (%)	ΔB (%)	ε$_{alt}$ (%)	Class
AP01	03 A/04A	DB	8	6	0.9994	-	57.4	56.8	-	57.9	1.0			B
		FC	8	7	0.9928	0.33–0.53	55.2	53.4	-	56.9	3.2			B
		DSC α 0.2	8	7	0.9866	0.33–0.53	50.7	49.1	-	52.4	3.3	14.2		B
		DSC α 0.5	8	7	0.9814	0.33–0.53	45.1	43.3	-	47.3	4.4	16.9	15.2	B
		DSC α 0.8	8	7	0.9763	0.33–0.53	39.0	37.0	-	41.1	5.3	18.5		B
AP04	03BI/AII	DB	7	7	0.9859	-	67.1	62.8	-	70.7	5.9			B
		FC	4	3	0.9958	0.38–0.46	63.7	58.3	-	71.7	10.5			B
		DSC α 0.2	4	4	0.9931	0.38–0.46	60.9	56.9	-	66.0	7.5	15.0		B
		DSC α 0.5	4	4	0.9893	0.38–0.46	55.4	50.3	-	62.3	10.8	17.6	11.0	B
		DSC α 0.8	4	4	0.9850	0.38–0.46	50.9	46.0	-	56.8	10.6	20.0		B
AP05	01B	DB	7	5	0.9406	-	117.5	45.5	-	181.1	57.7			-
		FC	4	4	0.8563	0.21–0.32	151.0	−748.1	-	913.6	550.2			-
		DSC α 0.2	4	4	0.9751	0.21–0.32	125.6	89.4	-	153.8	25.6	22.1		-
		DSC α 0.5	4	3	0.9991	0.21–0.32	100.4	96.7	-	104.1	3.7	23.6	5.4	B
		DSC α 0.8	4	3	0.9621	0.21–0.32	81.2	64.0	-	99.3	21.7	24.3		B
AP03	04A	DB	8	8	0.9968	-	28.6	27.6	-	29.7	3.7			B*
		FC	8	7	0.9981	0.21–0.32	27.7	26.4	-	28.7	4.2			B*
		DSC α 0.2	8	6	0.9976	0.21–0.32	25.0	24.2	-	25.8	3.2	30.8		B*
		DSC α 0.5	8	6	0.9957	0.21–0.32	22.0	21.1	-	23.0	4.3	30.4	15.7	B*
		DSC α 0.8	8	6	0.9935	0.21–0.32	18.8	17.6	-	19.9	6.1	37.0		B*
AP10	04A	DB	8	8	0.9935	-	32.4	30.9	-	33.7	4.3			B
		FC	8	6	0.9909	0.34–0.44	31.1	27.1	-	34.1	11.3			B
		DSC α 0.2	8	5	0.9950	0.34–0.44	28.8	26.5	-	30.5	6.9	13.6		B
		DSC α 0.5	8	6	0.9938	0.30–0.44	25.5	23.6	-	27.3	7.3	15.1	10.7	B
		DSC α 0.8	8	6	0.9938	0.30–0.44	23.8	22.1	-	25.2	6.5	17.1		B
AP12	07BII/CII	DB	7	6	0.7872	-	46.4	33.5	-	57.0	25.3			-
		FC	4	3	0.9988	0.24–0.35	49.9	47.6	-	52.0	4.4			A
		DSC α 0.2	4	4	0.9807	0.24–0.35	41.4	34.6	-	47.2	15.2	14.9		A
		DSC α 0.5	4	4	0.9830	0.24–0.35	36.8	31.1	-	41.6	14.3	17.2	7.2	A
		DSC α 0.8	4	4	0.9847	0.24–0.35	33.2	28.1	-	37.6	14.3	19.4		A
AP11	02A	DB	8	8	0.9687	-	21.9	17.8	-	26.1	18.9			-
		FC	8	6	0.9886	0.11–0.19	20.0	17.6	-	21.9	10.8			-
		DSC α 0.2	8	6	0.9976	0.11–0.19	17.5	16.8	-	18.1	3.7	26.5		-
		DSC α 0.5	8	6	0.9971	0.11–0.19	15.7	15.1	-	16.3	3.8	30.0	9.5	-
		DSC α 0.8	8	6	0.9961	0.11–0.19	14.3	13.8	-	14.9	3.8	33.1		-
AP14	06B	DB	7	6	0.9858	-	13.6	12.0	-	15.5	12.9			A
		FC	4	4	0.9998	0.47–0.48	14.4	14.1	-	14.6	1.7			A
		DSC α 0.2	4	4	0.9998	0.47–0.48	14.2	14.0	-	14.4	1.4	3.1		A
		DSC α 0.5	4	4	0.9992	0.47–0.48	14.0	13.5	-	14.4	3.2	3.7	2.6	A
		DSC α 0.8	4	4	0.9980	0.47–0.48	13.7	13.0	-	14.5	5.5	4.2		A
AP15	07 A/BII	DB	7	5	0.4624	-	52.8	−9.0	-	127.9	129.6			-
		FC	4	3	0.9649	0.10–0.18	27.1	11.7	-	36.7	46.1			-
		DSC α 0.2	4	3	0.9418	0.10–0.18	30.0	19.6	-	39.2	32.7	1.3		-

Table 3
Continued

Site	Spec.	Prot.	N	n	R^2	f-range	B (μT)	CI$_{95}$ (μT)		CI$_{95T/2}$ (%)	ΔB (%)	ε$_{alt}$ (%)	Class
		DSC α 0.5	4	3	0.9493	0.10–0.18	27.2	18.0	-	35.1	31.4	1.2	3.6	-
		DSC α 0.8	4	3	0.9552	0.10–0.18	24.9	16.7	-	31.7	30.1	1.3		-
AP17	06AII/BII	DB	7	6	0.9825	-	26.6	24.9	-	28.1	6.0			B
		FC	5	4	0.9887	0.18–0.33	25.6	22.0	-	28.5	12.7			B
		DSC α 0.2	5	5	0.9829	0.18–0.35	22.7	20.0	-	25.5	12.1	17.9		A
		DSC α 0.5	5	5	0.9822	0.18–0.34	19.9	17.1	-	22.4	13.3	20.5	8.0	B
		DSC α 0.8	5	5	0.9814	0.18–0.36	17.7	15.4	-	19.9	12.7	22.7		B
AP19	01BII/CII	DB	7	6	0.9946	-	26.2	25.5	-	26.9	2.7			-
		FC	5	4	0.9931	0.07–0.14	24.2	20.6	-	26.7	12.6			-
		DSC α 0.2	5	5	0.9792	0.07–0.14	21.6	18.6	-	24.4	13.4	17.0		-
		DSC α 0.5	5	5	0.9784	0.07–0.14	19.2	16.6	-	21.7	13.3	19.4	3.4	-
		DSC α 0.8	5	5	0.9775	0.07–0.14	17.3	14.7	-	19.7	14.5	22.2		-
AP20	07 B/09C	DB	8	7	0.9381	-	4.1	−10.8	-	22.0	403.9			-
		FC	8	4	0.9914	0.26–0.32	14.6	13.5	-	16.1	8.9			-
		DSC α 0.2	8	4	0.9759	0.26–0.32	12.7	10.9	-	15.2	16.9	46.5		-
		DSC α 0.5	8	4	0.9593	0.26–0.32	11.0	9.0	-	13.5	20.5	51.1	35.4	-
		DSC α 0.8	8	4	0.9424	0.26–0.32	9.7	7.6	-	12.5	25.3	54.7		-

Note. Site: Lava flow name. Spec.: Specimen sub-name. Prot.: MSP type protocol and Alpha (α) values applied. The determinations with the α value that generates the best linear fit are marked in bold, these results are selected to calculate the final average paleointensity. N: Number specimens with different B$_{lab}$ applied in the experiment. n: Number specimens with different B$_{lab}$ used in the determination. Experimental statistics: R^2, f-range, CI$_{95}$, ΔB and ε$_{alt}$ (Table 1). Class: Determination quality level; A represents determinations with higher quality; B*: Determination meets all criteria except ΔB. DSC, domain state correction protocol; FC, fraction correction.

We can see these results in Figures 2, 3, and S6 showing the MSP-DSC determination plots. The red line is the linear fit by means of weighted least squares of the Q$_{DSC}$ ratios (equation 17 in Fabian & Leonhardt, 2010), which vary in function of the alpha value used. The error bars of each point (representing specimens with different applied B$_{lab}$) are ΔQ$_i$, the alteration error plus the domain-state correction error (see equation 22 in Fabian & Leonhardt, 2010). The shaded area (anchored in (0, −1)) is delimited by the CI$_{95}$ of the best fitting lines. No pTRM is acquired if a null field is applied during the heating/cooling cycle, so that the linear fit must be anchored to the intercept (0,−1) (see Multispecimen Paleointensity online software http://ambre.gm.univ-montp2.fr/camps/MSP_DSC/). The weights are taken as the inverse of the intrinsic errors ΔQ$_i$ of each measurement.

In previous works, an overestimation of DB over DSC paleointensities of up to 20% had been observed (e. g. Calvo-Rathert et al., 2016; Fabian & Leonhardt, 2007; Michalk et al., 2008, 2010). Our results also confirm this overestimation in most of the determinations, except in AP20 where DSC > DB and AP14 where DB and DSC are indistinguishable.

Another interesting result is arised from MSP determinations carried out over specimens from two different cores in a same lava flow (Table 3). AP01 (cores 03 and 04) passes the proposed MSP quality criteria and the paleointensity obtained agrees with IZZI using TTP criteria, although it differs from that obtained with Thellier-Thellier (TT) and TTP criteria (Table 4). AP20 (cores 07 and 09) does not pass the MSP quality criteria and the result coincides with those obtained with both Thellier-type methods under both sets of criteria (TTP and RCRIT). No behavioral pattern is observed in which the use of distant specimens shows any influence. In both cases, the paleointensities follow the trend of the Thellier-type determinations and the MSP quality criteria may or may not be met, as in the other MSP-DSC determinations. These determinations will be treated in the same way as those carried out on specimens from the same sample when we calculate the final paleointensities averaged by lava flow.
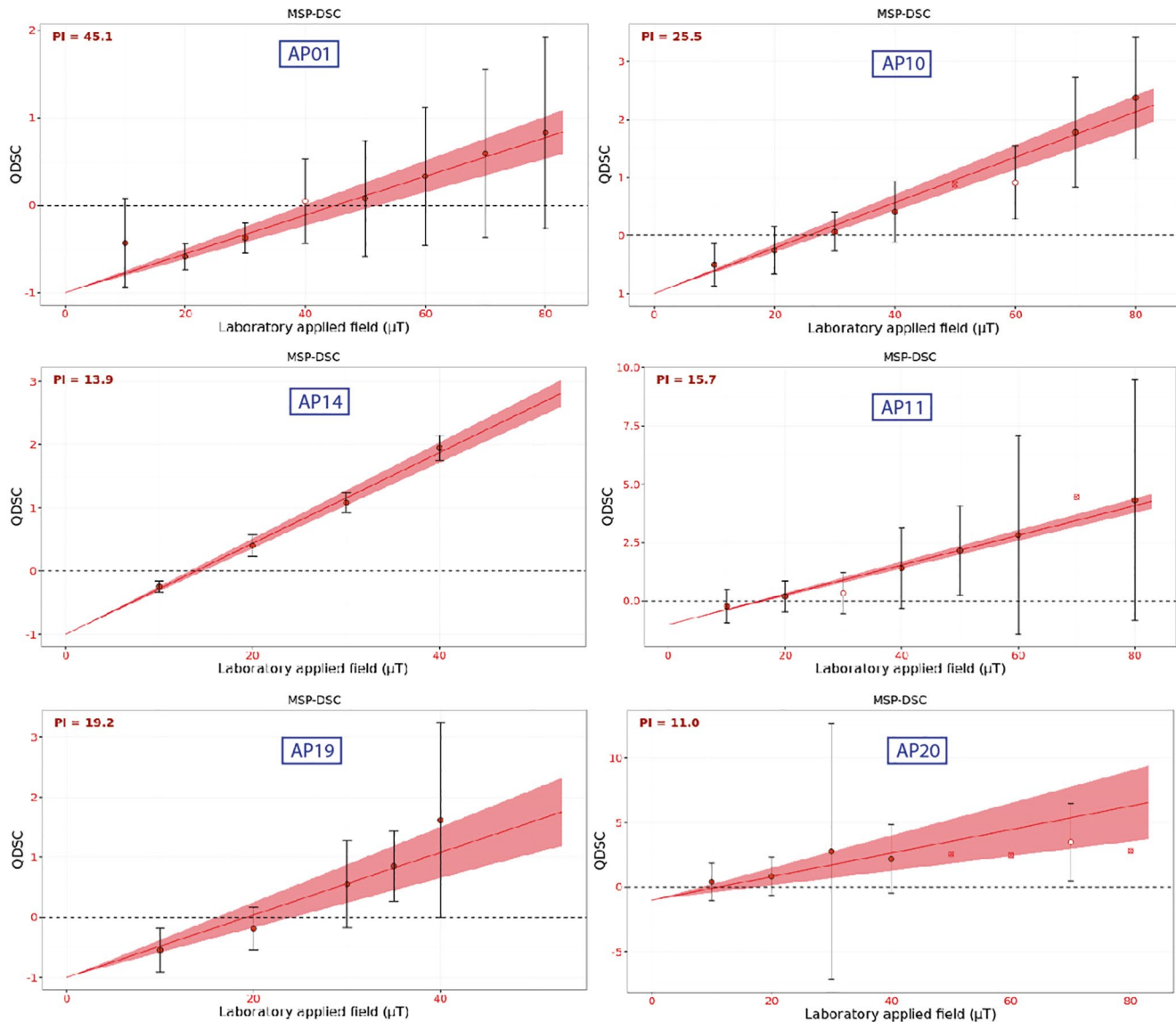
Figure 2. MSP-DSC paleointensity determination plots obtained by the MultiSpecimen Paleointensity online software (http://ambre.gm.univ-montp2.fr/camps/MSP_DSC/). AP01, AP10 and AP14 belong to successful determinations, assigned to quality levels of class B, B and A, respectively (see Table 3). AP11, AP19 and AP20 are failed determinations. Their results agree with the Thellier-type ones but show a very low f range in the first two cases or very high ϵ_{alt} and ΔB values in the case of the latter one (see Table 3). Closed (open) symbols represent data used (rejected) in the paleointensity determination; each of these points is the Q_{DSC} ratio (equation 17 in Fabian & Leonhardt, 2010) from each specimen to which a different B_{lab} has been applied; Q_{DSC} vary on function of the α used. The error bar for each point is ΔQ_i (equation 22 in Fabian & Leonhardt, 2010), the absolute error sum of the alteration and correction of the state of domains. The weights are taken as the inverse of the intrinsic errors ΔQ_i of each measurements. The shaded area (anchored in (0, −1)) is delimited by the CI_{95} of the best fitting line. For physical reasons, i.e., no pTRM is acquired if a null field is applied during the heating/cooling cycle, the linear fit must be anchored to the intercept (0,−1). MSP-DSC: Multispecimen domain-state correction; pTRM, partial thermoremanent magnetization.

5.3. Thellier-Type Paleointensities with TTP Selection Criteria

Paleointensity determinations performed in the previous work of Sánchez-Moreno et al. (2020) with the Thellier-Thellier (TT) and IZZI methods (Thellier and Thellier, 1959; Yu et al., 2004) and interpreted with the rather strict set of selection criteria RCRIT (Tauxe et al., 2016) have been reinterpreted in the present study. In order to carry out an analysis of the influence of the selection criteria on the results, a more flexible set of TTP criteria (Leonhardt et al., 2004 modified by; Paterson et al., 2014a, 2014b) has been applied in the reinterpretation. In this section, we will compare the results of the Thellier-type determinations under both
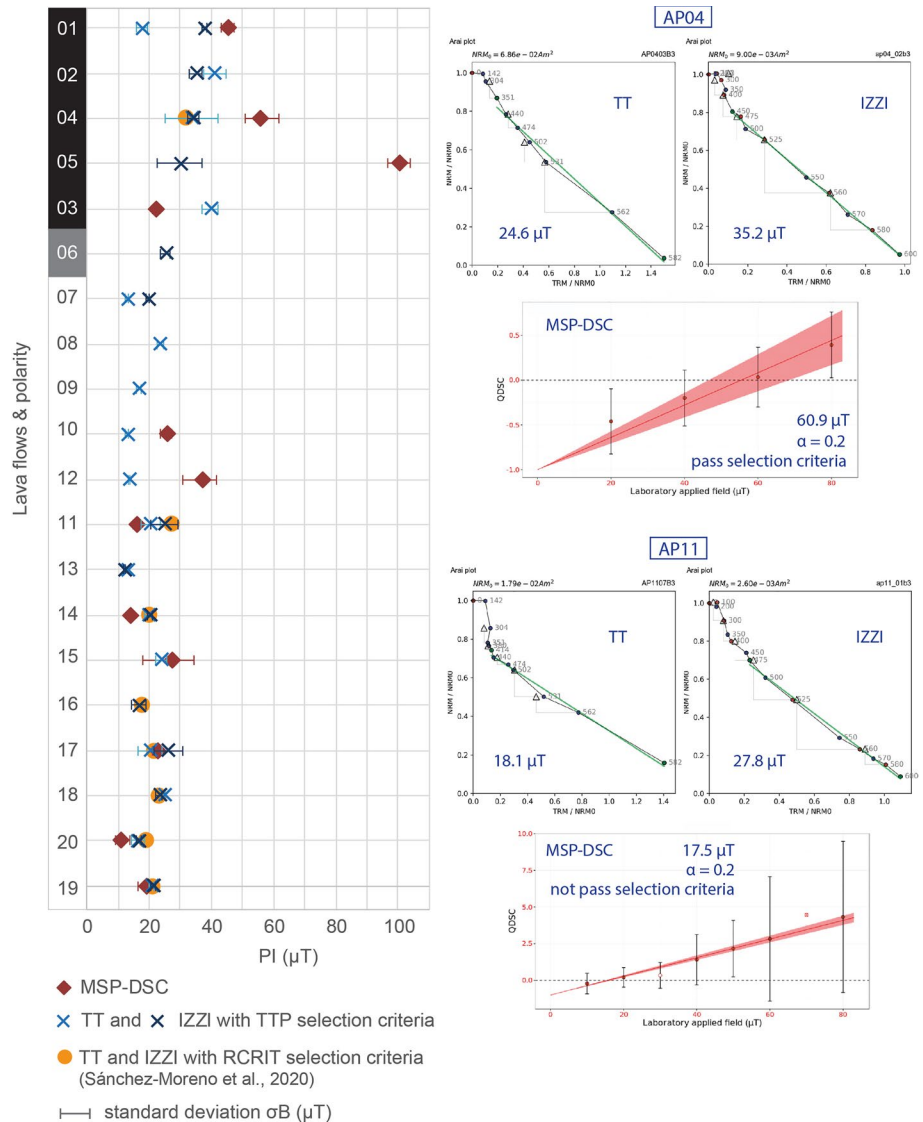
Figure 3. (a) Paleointensities per lava flow obtained in the Apnia sequence by multispecimen with domain-state correction (MSP-DSC) (Fabian & Leonhardt, 2010) and Thellier-Thellier method (TT; Thellier and Thellier 1959) and IZZI method (Yu et al., 2004) applying TTP (based on Paterson et al., 2014a, 2014b) and RCRIT (Tauxe et al., 2016) selection criteria. MSP-DSC results are plotted whether they pass the proposed selection criteria or not. (b) and (c) Experimental examples from AP04 and AP11 lava flows are shown. TT and IZZI plots interpreted with TTP criteria. MSP plots: closed (open) symbols represent data used (rejected) in the paleointensity determination; each of these points is the Q_{DSC} ratio from each specimen to which a different B_{lab} has been applied; the error bars are the ΔQ_i error; the red line is the linear fit of Q_{DSC} values by weighted minimum squares regression; the shaded area (anchored in (0, −1)) is delimited by 95% Confidence Intervals (CI$_{95}$) of the best fitting lines. In the case of AP04, MSP-DSC passes the proposed criteria (Table 3) but the paleointensity value does not match that obtained in the Thellier-type methods. AP11 shows the opposite case, MSP-DSC does not pass the criteria although paleointensities agree. IZZI, In-field/Zero-field protocol.

sets of criteria TTP and RCRIT. In section 6.1, we will compare the two sets of Thellier type results with the MSP-DSC results. Finally, in section 6.3 we will compare the paleointensity averages obtained from MSP-DSC plus the two sets of Thellier-type results separately.

Results under TTP criteria have been obtained for the 20 lava flows of the sequence (Table 4, S2 and S3). In 11 flows, we can add three or more determinations per flow from both methods TT and IZZI. Four flows yield three or more determinations by a single method. In five flows, only one or two determinations have

Table 4
Paleointensity Averaged For Each Lava Flow And For Different Absolute Paleointensity Determination Methods And Quality Criteria

| | RCRIT criteria Sánchez-Moreno et al. (2020) | | | TTP criteria | | | | | | MSP-DSC | | | | | | | | |
| | TT + IZZI | | | TT | | | IZZI | | | α = 0.2 | | | α = 0.5 | | | α = 0.8 | | |
Site	N	B (µT)	σB (µT)	n	B (µT)	σB (µT)	n	B (µT)	σB (µT)	n	B (µT)	95% CI$_{T/2}$ (µT)	n	B (µT)	95% CI$_{T/2}$ (µT)	n	B (µT)	95% CI$_{T/2}$ (µT)
AP01				2	17.8	1.8	1	37.8	0.8	7	50.7	1.7	7	45.1	2.0	7	39.0	2.1
AP02				2	41.0	3.5	4	35.1	2.1									
AP04	5	32.1	3.3	3	33.5	8.4	4	34.1	1.7	4	60.9	4.6	4	55.4	6.0	4	50.9	5.4
AP05							4	29.9	7.3	4	125.6	32.2	3	100.4	3.7	3	81.2	17.7
AP03				1	39.6	2.4				6	25.0	0.8	6	22.0	0.9	6	18.8	1.2
AP06							3	25.2	1.6									
AP07				1	12.9	0.5	2	19.6	0.5									
AP08				1	23.6	1.1												
AP09				3	16.6	0.7												
AP10				2	12.9	0.6				5	28.8	2.0	6	25.5	1.9	6	23.8	1.6
AP12				2	13.6	0.4				4	41.4	6.3	4	36.8	5.3	4	33.2	4.8
AP11	3	26.8	4.0	2	20.3	3.1	4	24.9	4.6	6	17.5	0.7	6	15.7	0.6	6	14.3	0.6
AP13				1	13.0	0.7	2	12.2	0.2									
AP14	8	19.8	0.4	3	19.6	1.3	6	20.3	0.7	4	14.2	0.2	4	14.0	0.5	4	13.7	0.8
AP15				1	23.9	1.6				3	30.0	9.8	3	27.2	8.6	3	24.9	7.5
AP16	5	16.8	2.4				5	16.8	2.3									
AP17	6	22.7	4.3	2	20.2	4.0	7	26.1	4.7	5	22.7	2.8	5	19.9	2.7	5	17.7	2.3
AP19	5	21.0	0.7	2	20.9	0.8	5	21.3	1.0	5	21.6	2.9	5	19.2	2.6	5	17.3	2.5
AP18	5	24.1	0.4	1	24.7	0.5	4	23.1	1.1									
AP20	3	19.4	0.2	3	16.4	1.9	3	16.8	0.8	4	12.7	2.2	4	11.0	2.3	4	9.7	2.5

Note. All the paleointensities obtained by the multispecimen method are shown, even if the quality criteria are not fulfilled. n: Number of specimens used in the determination. B: Paleointensity. CI$_{95T/2}$: 95% confidence interval divided by two. σB: standard deviation. TT: Thellier-Thellier (1959). IZZI: In-field Zero-field protocol (Yu et al., 2004). MSP-DSC: Multispecimen with Domain-State Correction (Fabian & Leonhardt, 2010). TTP: quality criteria based on Leonhardt et al. (2004) modified by Paterson et al. (2014a, 2014b). RCRIT: Strict quality criteria used in Sánchez-Moreno et al., 2020 based on Tauxe et al. (2016). α: Alpha parameter values applied to MSP-DSC. MSP-DSC results in bold and underlined indicate the best linear fit obtained with a given α, these results are used in the final average lava flow paleointensity.
MSP-DSC, multispecimen - domain state correction protocol.

been obtained from a single method. With less than three determinations, the average per lava flow will not be calculated and will not be compared with the MSP-DSC results.

The paleointensities under TTP in the upper normal polarity part vary between 29.9 and 41 µT, except AP01 with 17.8 µT from two TT determinations. In flow AP01, one IZZI determination of 37.8 µT was also obtained. Both two TT determinations in AP01 show a lower f parameter value and a higher |k'| than the IZZI one. This TT result will not be taken to calculate the flow intensity average. The AP06 transitional polarity flow gives 25.2 µT from three IZZI determinations. The reverse polarity section shows lower values, between 12.2 and 26.1 µT.

If we compare these results with those obtained in Sánchez-Moreno et al. (2020) with the RCRIT criteria, we can see very similar paleointensity values for each section of different polarity. In the upper normal polarity section one flow of 32.1 µT and in the reverse polarity ones seven results from 16.8 and 26.8 µT.

Both interpretations show the same behavior pattern throughout the sequence: First a reversal polarity section of low paleointensities, followed by a normal polarity section with higher paleointensities. However,

the intensity difference observed between the two sections of different polarity is lower with RCRIT results than with TTP ones.

6. Discussion

6.1. MSP-DSC Versus Thellier-Type

In this section, the intensity values obtained with the MSP-DSC method will be analyzed against those obtained with the Thellier-type methods (TT and IZZI), under the RCRIT (Sanchez-Moreno et al., 2020) and TTP (used for reinterpretation in this study) criteria sets. For this comparison, and later calculation of the final flow-average paleointensities (section 6.3), only the results from MSP-DSC protocol will be used, since as noted in section 5.2, it corrects the overestimation in the paleointensity values produced by MSP-DB. Besides, we have taken the MSP-DSC paleointensities yielded by the α parameter (0.2, 0.5 or 0.8) which shows the highest R^2 coefficient in the linear regression of the determinations. For this comparison, we assume that TT, IZZI and MSP-DSC mean paleointensities agree if the standard deviation (sd) between them is ≤ 25% (Biggin & Paterson, 2014).

The study carried out by Sánchez-Moreno et al. (2020) used RCRIT criteria and yielded results in eight lava flows, where the averages have been calculated from three or more determinations. The TTP criteria set yields results in 15 different lava flows averaging three or more determinations (Table 4). TTP also gives results on five lava flows with only one or two determinations. Paleointensity results in flows with both RCRIT and TTP agree with both interpretations. Likewise, RCRIT and TTP paleointensities show the same similarities and differences with MSP-DSC (Table 4 and Figure 3). Since RCRIT and TTP paleointensities are similar in those flows where both approaches have yielded results, the detailed comparison with MSP-DSC will be done with the TTP results, since they are available for a greater number of flows to detect different types of behavior (Tables 4 and 5 and Figure 3):

Case 1: Good technical quality MSP-DSC paleointensities agree with Thellier-type ones (sd < 25%): Flows AP01, AP04, AP14 and AP17.

For flow AP01, specimens from two different samples (03A and 04A) have been used in the MSP-DSC determination. In a specimen of the same sample 03A, an IZZI determination with a concave-up shape Arai plot was detected indicated presence of MD grains. Specimen 04 A, on the other hand, shows a linear-shape Arai plot (SD grains), but a mixture SD + MD trend in the Day-plot (Sánchez-Moreno et al., 2018), which can also be interpreted as PSD/Vortex. In this case, it can be checked that the domain state correction works correctly, as these samples have mixture SD + MD behavior.

In AP04, AP14 and AP17, we observed successful MSP-DSC and TT determinations, in specimens of the same core. In addition, for the whole sequence, the hysteresis parameters fall into the SD + MD box. The proportion of SD grains could be higher in these samples, allowing successful paleointensity determinations with both methods of determination

Case 2: Good technical quality MSP-DSC paleointensities disagree with Thellier-type ones: Flows AP05, AP03, AP10 and AP12.

The MSP-DSC determination in AP05 yields a substantially higher paleointensity of 100.4 μT (from three specimens of core 01). This is a contradictory behavior because results meet quality criteria but the paleointensity value is inconsistent. The average value from four IZZI determinations in AP05 is 30 μT. The hysteresis parameters from a specimen contiguous to the one used for the MSP-DSC determination shows a SD + MD trending behavior in the Day-plot. Successful IZZI determinations come from cores 02 and 06, but another specimen from core 01 displays a concave-up-shaped Arai plot. Therefore, we have a concave-up Arai, a SD + MD trend from hysteresis parameters and a successful but high value MSP-DSC paleointensity from very close specimens. This means that the proportion of particles that behave as PSD/vortex in the specimen selected for MSP-DSC (core 01) is higher than the ones selected for IZZI (cores 02 and 06).

Table 5
Final Weighted Average Paleointensities per Lava Flow In The Apnia Sequence

Age (Ma)	Site	no determinations TTP TT	IZZI	MSP DSC	Q	B (μT)	sd (μT)	sd (%)	VADM (10²² Am²)	σVADM (10²² Am²)	no determinations RCRIT TT	IZZI	MSP DSC	Q	B (μT)	sd (μT)	sd (%)	VADM (10²² Am²)	σVADM (10²² Am²)
3.09	AP01	+	1	1	1	44.3	9.1	20.6	7.5	1.55	x	x	1						
	AP02	2	4	-	2	37.1	3.0	8.2	6.3	0.51	x	x	-						
	AP04	3	4	1	1	37.2	9.6	25.7	6.3	1.63	1	4	1	1	36.9	11.8	31.9	6.3	2.00
	AP05	x	4	1		44.0	31.5	71.7	7.5	5.36	x	x	1						
3.28	AP03	1	x	1		32.3	10.3	32.0	5.5	1.75	x	x	1						
	AP06	x	3	-							x	x	-						
	AP07	1	2	-	2	17.4	3.9	22.3	3.0	0.66	x	x	-						
3.75	AP08	1	x	-							x	x	-						
	AP09	3	x	-							x	x	-						
	AP10	2	x	1		18.2	9.2	50.4	3.1	1.57	x	x	1						
3.70	AP12	2	x	1		20.1	11.3	56.2	3.4	1.92	x	x	1						
	AP11	2	4	1	2	23.4	2.4	10.2			x	3	X	3	26.8	4.0	14.4	4.6	0.68
		2	4	1		22.5	3.1	13.8	3.8	0.53	x	3	1		24.5	4.6	19.0	4.2	0.79
	AP13	1	2	-	2	12.5	0.5	3.7	2.1	0.09	x	x	-						
	AP14	3	6	1	1	19.5	1.9	9.7	3.3	0.32	2	6	1	1	19.2	1.9	9.7	3.3	0.32
	AP15	1	x	x							x	x	X						
		1	x	1		24.4	0.7	2.9	4.2	0.12	x	x	1						
	AP16	x	5	-							x	5	-	3	16.8	2.4	14.3	2.9	0.41
	AP17	2	7	1	1	24.6	2.5	10.3	4.2	0.43	x	6	1	1	22.7	0.0	0.0	3.9	0.00
	AP19	2	5	x	2	21.2	0.2	0.9	3.6	0.03	x	5	x	3	21.0	0.7	3.2	3.6	0.12
		2	5	1		21.2	0.2	1.1	3.6	0.03	x	5	1		21.1	0.2	1.2	3.6	0.04
	AP18	1	4	-	2	23.4	0.7	3.1	4.0	0.12	1	4	-	2	24.1	0.4	1.8	4.1	0.07
	AP20	2	3	x	2	16.6	0.2	1.3	2.8	0.03	x	3	x	3	19.4	0.2	0.1	3.3	0.03
		2	3	1		16.0	1.5	9.3	2.7	0.26	x	3	1		17.7	3.4	18.9	3.0	0.57

+		rejected by low quality determinations
-		not measured
X		rejected by not passing criteria

Note. Final weighted paleointensity average calculated by lava flow using the number of individual determinations (note that in the case of multispecimen determinations, although several specimens are used for a single determination the weighted value remains equal to 1). The number of determinations performed with each method is shown. Those methods rejected by paleointensity value, or quality criteria or those not measured are indicated. Q: quality category of the paleointensity average. TT: Thellier-Thellier (1959); IZZI, In-field/Zero-field protocol (Yu et al., 2004); MSP-DSC, Multispecimen domain-state correction (Fabian & Leonhardt, 2010). TTP, quality criteria based on Leonhardt et al. (2004) modified by Paterson et al. (2014a, 2014b). RCRIT, Strict quality criteria used in Sánchez-Moreno et al., 2020 based on Tauxe et al. (2016). VADM, Virtual axial dipole moment. σVADM, Virtual axial dipole moment error calculated from *sd* (μT).

In AP03, a single TT determination yields a higher paleointensity value (39.6 μT, core 02) than the MSP-DSC result (22 μT, core 04) obtained from six specimens. AP10 and AP12 have the opposite behavior than the previous flows. Thellier-type experiments (two determinations per flow) yield low paleointensities if compared to MSP-DSC (with six and four specimens, respectively). In these three flows a SD + MD tendency is observed, which could also point toward PSD/vortex and SD behavior in different close specimens. In other words, different behaviors can be observed in very close samples, as the grain size varies a lot in a small space.

Case 3: Bad technical quality MSP-DSC paleointensities agree with Thellier-type ones. AP11, AP15 and AP19 do not fit the MSP quality criterion $f < 0.2$, AP15 also shows a high CI_{95} value and AP20 shows strong alteration with $_{alt} = 35.4$ %.

In these four flows, we find successful Thellier-type determinations in specimens from the same core or very close to that used in MSP, together with the SD + MD trend observed in the sequence. These could be specimens with a higher SD content. The high uncertainties in MSP can be caused by instrumental problems as a low applied temperature or too few B_{lab} steps close to the paleointensity result.

AP20 shows a high alteration in MSP-DSC, but reversible Ms-T curves (cores 01, 04, 08). The experiment has been carried out over specimens from different cores (07 and 09). Perhaps the corrections have not compensated the difference in the NRM fraction used or in the domain-state? A precise pattern cannot be recognized.

6.2. Quality Criteria in the MSP Method

MSP-DSC results calculated with an α parameter that produces the best linear fit have been selected. Different Alpha (α) values optimize MSP-DSC paleointensity results depending on mineralogy and grain size of the samples and temperature applied in the determinations. In six determinations, the best result is obtained with $\alpha = 0.2$, in one with $\alpha = 0.8$ and in another one with $\alpha = 0.5$ (Table 3). If we observe the thermal behavior in the demagnetization and Ms-T curves or their hysteresis parameters (Sánchez-Moreno et al., 2018) from close specimens, we do not appreciate differences that produce better results when α varies. However, the results from α with the best linear fit show lower CI_{95}, ΔB and $\mathcal{E}_{alt}$ values. It could be pointed out that a low α works better in the Apnia sequence.

The fraction parameter f (Fabian & Leonhardt, 2010) is the ratio between the fraction of NRM removed and overprinted by the laboratory pTRM in each specimen subjected to different B_{lab}. The commonly proposed threshold values lie between 0.2 and 0.8 (20%–80% of the full NRM). In this range, the fraction is large enough to be precisely measured but still clearly below a full NRM (Tema et al., 2016). It is obtained from the half vector sum between measurements m1 and m2 of the MSP-DSC procedure (Tables 1 and S1) normalized by the NRM, hence it can only be calculated for the FC and DSC determinations. Even so, we consider that it is also applicable to the original MSP-DB method, because it depends on the temperature reached during the experiment (and therefore on the amount of TRM unblocked and overprinted), which in the three MSP variants is the same. In the present study, we decided to apply 450°C to all samples (section 4.2), but in some determinations, f is less than 0.2 (Table 3). In such cases, a higher temperature would have been more adequate, since the magnetization drop in these samples occurs at slightly higher temperatures, and the f-range used in the MSP experiments is sensitive to the temperature applied. Comparison with Thellier-type experiments, however, shows that the MSP-DSC determinations in which $f < 0.2$ (AP11, AP15 and AP19) yield similar paleointensities (Table 4 and Figure 3). This observation may indicate that a lower f range is valid in some specific MSP determinations. A possible explanation could be that the fraction correction (MSP-FC step) compensates the low proportion of the NRM used in some of the specimens of these determinations. However, when we observe the thermal demagnetization behavior in samples of the same core and close to those used in MSP-DSC with results $f < 0.2$, they keep between 20% and 30% of the NRM at 450°C. This value is relatively near to the 20% threshold, but theoretically sufficient to carry out the determination successfully. Therefore, we have no clear interpretation of why these samples produce paleointensity values similar to Thellier-type using such a low f ratio.

The relative alteration error ε_{alt} (Fabian & Leonhardt, 2010) is calculated with measurement m1 and repeated measurement m4 of the of the MSP-DSC procedure (Tables 1 and S1). As it is considered that for thermo-chemical changes the temperature attained is more important than the number of heatings, it is possible to use ε_{alt} for all MSP variants. Monster et al., (2015a, 2015b) have proposed a possibly too strict threshold $\leq 3\%$, which is used by Calvo-Rathert et al., (2016), while Tema et al., (2016) suggest a 10% threshold in what they consider a strict criteria set. A more flexible approach is that proposed later by Carvallo et al. (2017), who take $\varepsilon_{alt} \leq 20\%$. In this work, we will apply the 10% threshold for class A and a 20% one for class B determinations. Only the AP20 flow shows a really high $\mathcal{E}_{alt}$ value of 35.4%, clearly above the more

flexible proposed limit (Table 3). However, the MSP-DSC paleointensity obtained is close to that obtained with the Thellier-type methods (Table 4). In addition, the Ms-T curves performed in this flow show reversible thermal behaviors (Type H), i.e., without alterations (Figure S4 and S5). This suggests that the magnetic properties in these materials can vary significantly between very close specimens.

Parameters ΔB (ΔH from Fabian & Leonhardt, 2010) and CI_{95} provide an estimation of the uncertainty. ΔB is the final error of the determination obtained by the total error of each specimen used in the determination (see ΔQ_i in Table 1). To find out ΔB, the alteration-induced error (which includes ε_{alt}) and the approximation of the absolute error of the domain-state correction are calculated. Like the relative alteration error ε_{alt}, ΔB also depends on the temperature reached, and hence it may be considered to evaluate the quality of DB and FC determinations as well as those of the DSC. CI_{95} is the bootstrapped 95% confidence interval calculated and critically evaluated with the Shapiro-Wilk test of normality (see Multispecimen Paleointensity 1.5. software online version http://ambre.gm.univ-montp2.fr). An almost ideal determination is achieved when the upper and lower limits are symmetrical with respect to the paleointensity value. In the present study, the results provided in several cases by CI_{95} and ΔB are contradictory. In such cases, only the CI_{95} parameter is taken into account.

AP15 shows rather high CI_{95} values (Table 3), compared to the remaining flows in which MSP-DSC has been performed. If we observe the Ms-T curve recorded in the same core 07 (Figure S4), it presents a reversible behavior (Type H), while during thermal demagnetization 30% of the NRM still is kept at 450°C. The Thellier-type determination carried out on core 07 passes the TTP criteria, and the paleointensity value obtained are similar to MSP-DSC one. In this case, there is also no clear correlation between the CI_{95} parameter and the paleointensity result and magnetic properties of the analyzed sample.

Finally, when we compare paleointensities from MSP-DSC that do not pass the criteria with Thellier-type ones (applying both selection criteria sets, TTP and RCRIT), like in case 3 in section 6.1, we obtain similar paleointensities (Tables 4 and 5). This may lead us to think that the thresholds of the MSP selection criteria proposed can be applied in a more flexible way. However, in this work we are going to keep the initial criteria, because to support this affirmation it is necessary to observe this behavior in a greater number of results.

6.3. Paleointensity Average Per Lava Flow

In order to achieve highly reliable paleointensities by combining the results of different methods (i.e., a multi-method approach), the following guidelines have been applied to Thellier-Thellier, IZZI and MSP results:

(i) Results of both Thellier-type and MSP determinations are obtained after applying specific selection criteria.

(ii) Agreement of paleointensity results from MSP and Thellier-type determinations is considered as an added strong indicator of a successful paleointensity result, as a match obtained from two failed experiments performed with different methods can be considered highly unlikely.

(iii) Average paleointensity between IZZI and TT method is also considered a strong reliability marker, although lower than the MSP with TT and/or IZZI agreement ((ii) guideline).

Besides, the MSP-DSC protocol with domain-state corrections is considered more reliable than the MSP-DB without corrections. Thereupon, the paleointensities deployed in the multi-method approach are going to be the ones yielded by MSP-DSC. Regarding the uneven behavior in some results, it should be borne in mind that MSP is a new method with discrepancies between different authors regarding the quality criteria and their threshold values (section 6.1).

Mean paleointensities have been weighted according to the number of determinations of each method (Tables 4 and 5), and the valid average paleointensity per flow must have a standard deviation value within ±25%. According to the methods involved in the average, two quality levels can be distinguished. The averaged results for the MSP-DSC together with the Thellier-type results re-interpreted in the present study with TTP criteria (Paterson et al., 2014a, 2014b), will be presented below.

Quality 1: Average paleointensity per lava flow calculated with at least one Thellier-type determination and one good quality MSP-DSC determination. Flows AP01, AP04, AP14 and AP17 present the most reliable paleointensities (Table 5). The agreement of MSP-DSC and Thellier-type results enhances the reliability of these data.

AP01, however, yields 17.8 µT from 2 TT determinations, while in this same flow one IZZI determination of 37.8 µT is obtained. Both 2 TT determinations in AP01 show a lower f parameter value and a higher |k′| than the IZZI one. For this reason, this TT result has not been used in the calculation of intensity average per flow

Quality 2: Both TT and IZZI determinations comprise the average and in total, they must add up to at least three determinations: Flows AP02, AP07, AP11, AP13, AP19, AP18 and AP20 (Table 5).

Mean paleointensities have been obtained for 11 out of 20 flows that comprise the Apnia sequence (Table 5 and Figure 3) from Thellier-type methos under TTP criteria and MSP-DSC. Four paleointensities belong to quality level 1 and 7 to quality 2. Paleointensity values in the lower reverse polarity section range between 12.5 and 24.6 µT. In the upper normal polarity section, the paleointensities show higher values, which range between 37.2 and 44.3 µT (Table 4).

Four MSP-DSC determinations have not been formally considered reliable (Table 3). Even so, we have also calculated the paleointensity averages by flow including them to observe differences and similarities (italics in Table 5) between both calculations. When we include MSP-DSC in AP11, AP19 and AP20 we obtain similar paleointensity values to those obtained with Thellier-type determinations (TTP criteria). In AP15 we only have one TT paleointensity of 23.9 µT, while MSP-DSC is 24.9 µT. In addition, the results are similar when we compare them with Thellier-type applying RCRIT criteria.

If we now perform the same type of average between Thellier-type and MSP results, but now using the results obtained in Sánchez-Moreno et al. (2020) for Thellier-type data obtained with RCRIT criteria, we obtain three results of quality 1, AP04, AP14 and AP17 and 1 of quality 2, AP18. Again, paleointensity values are lower in the reverse polarity section than in the normal polarity one.

We have added a third quality level (Q3 in Table 5: AP11, AP16, AP19 and AP20) to classify the Thellier-type determinations that come from a single method, TT or IZZI, and to which the set of RCRIT criteria has been applied (Sánchez-Moreno et al., 2020). Although in this quality level only determinations obtained from a single method are considered, RCRIT criteria provide a high reliability due to their degree of strictness, which only accepts the results with higher quality.

Biggin and Paterson (2014) suggest that a site-average must include paleointensities from more than one technique to support results of high reliability. In addition, they put forward a new collection of basically qualitative reliability criteria for paleointensity results at the site mean level, which they label Q_{PI}. They intend to identify biasing agents applicable to paleointensity measurements, which are sometimes obviated, to quantify the reliability of the paleointensity values obtained from a study. The Q_{PI} criteria applied to our results (paleointensities of quality (Q) 1 and 2 in Table 5) are the following:

1. AGE: Reliable age and primary component of remanence. Apnia paleointensity results show a reliable age and paleomagnetic behavior originating from a primary component of remanence.
2. STAT: A minimum of five individual sample estimates per unit with low dispersion (true SD/mean ≤ 25%; Paterson et al., 2010). Nine lava flows fulfill the condition of five individual specimens used in the paleointensity average (AP01, 02, 04, 11, 14, 17, 19, 18 and 20) in the comparison with Thellier-type under TTP criteria results. AP07 and AP13 only include 3 determinations (from TT and IZZI). On the other hand, under RCRIT, all paleointensity averages fulfill the requirement (AP04, AP14, AP17 and AP18).
3. TRM: Microscope analysis supports the evidence that the remanence is a thermoremanence.
4. ALT: pTRM checks and rock magnetism experiments (also the ε_{alt} parameter in MSP determinations) support that there is not alteration.
5. MD: A high f parameter in Thellier-type and the domain state correction in MSP-DSC determinations validate that the effect of MD grains does not influence the final paleointensity estimate.
6. ACN: Anisotropy of TRM, Cooling rate and Non-linear TRM effects.
   - Anisotropy of TRM: Anisotropy of magnetic susceptibility (AMS) was measured on one sample from each flow showing low corrected anisotropy P′ (Jelinek, 1981) values between 1.000 and 1.040

(average 1.014; Sánchez-Moreno et al., 2020). The gamma statistic γ (Paterson et al., 2014a, 2014b) in both IZZI and Thellier-Thellier determinations yields low values between 0.2° and 3.7°. Samples are considered to have higher chance to be anisotropic only when $\gamma >> 4°$ (Paterson et al., 2015).

- Cooling rate: Characteristics of the flows like thickness or composition suggest that paleointensity experiments are not affected by the cooling-rate, because they do not vary significantly in the individual cooling units. Samples have been cooled under natural conditions (∼10 h) in the Thellier-Thellier experiments and with a fan (∼1 h) in the IZZI experiments and (Sánchez-Moreno et al., 2020), without differences in the results.

- Non-linear TRM effects: They are minimal when the laboratory and ancient field strengths are approximately equal (Paterson, 2013; Selkin et al., 2007). For most typical geological materials (i. e., lavas), if both fields are within ∼1.5 times each other, the influence of non-linear TRM is likely to be minimal (Biggin & Paterson, 2014).

7. TECH: Final paleointensity from 11 flows has been obtained using results from more than one technique in averages with MSP-DSC and Thellier-type with TTP criteria and four from RCRIT one.

8. LITH: The paleointensity estimations have been obtained on samples of similar lithology and unblocking behavior.

From this analysis nine final mean paleointensities (MSP-DSC and Thellier-type with TTP) can be classified as $Q_{PI} = 7$ (lava flows AP01, 02, 04, 11, 14, 17, 19, 18 and 20). AP07 and AP13 show a $Q_{PI} = 6$. Results of the comparison of MSP-DSC and Thellier-type with RCRIT show $Q_{PI} = 7$ (AP04, AP14, AP17 and AP18). All the final paleointensities obtained in this work show a high Q_{PI} value, indicating a high reliability of the data.

6.4. Directional Results Versus Paleointensities

Paleomagnetic directions obtained in the Apnia sequence can be consistent with a record of a polarity reversal (Sánchez-Moreno et al., 2018). Radiometric ages (Lebedev et al., 2008) suggest that the record may correspond either to the Gilbert-Gauss reversal (C2Ar to C2An-3n) or to a combined transition register from C2Ar to C2An-2n subchrons (Figure S3). Moreover, Sánchez-Moreno et al. (2018) concluded that the analysis of paleomagnetic directions in combination with the virtual geomagnetic pole scatter and some earlier paleointensity results (Calvo-Rathert et al., 2013), enable two non-exclusive interpretations: An anomalous EMF record or a short recording time unable to average paleosecular variation. The flow-average paleointensities obtained in the present study yield a range of VADMs (Virtual Axial Dipolar Moments) from 2.1 to 4.2×10^{22} Am^2 in the reverse-polarity lower section, while the upper normal-polarity section provides higher values between 6.3 and 9.1×10^{22} Am^2.

During large departures of the geomagnetic field from the GAD, the intensity decreases significantly (e.g., Laj & Channell, 2007 and references therein). Furthermore, the intensity variation begins before the direction variation (Herrero-Bervera & Valet, 1999; Prévot, Mankinen, Coe, Grommé, 1985, Prévot, Mankinen, Grommé, Coe, 1985; Riisager et al., 2000). After the directional change, the intensity increases rapidly above the previous values in a rebound effect, after which it stabilizes. Besides, the Time-Averaged Field (TAF) value for the last 5 Ma, according to different authors, varies between 4.1 and 5.6×10^{22} Am^2 (Cromwell et al., 2015b; Juárez and Tauxe, 2000; Lawrence et al., 2009; Wang et al., 2015). For larger periods such as the last 160, 200, and 300 Ma, TAF is estimated between 4.2 and 4.8×10^{22} Am^2 (Calvo-Rathert et al., 2020; Juárez et al., 1998; Selkin and Tauxe, 2000; Tauxe 2006; Tauxe et al., 2013). All these observations allow to infer that the lower Apnia section records the initial stage of a reversal while the upper part of the sequence displays the recuperation of the EMF intensity following the polarity transition. The multi-method approach applied in the present study provides consistent paleointensity support to the previous directional interpretation of the record as a polarity reversal.

7. Conclusions

An inter-laboratory and multi-method absolute paleointensity determination study has been performed on the 20 flows forming the Pliocene Apnia lava flow sequence in the Lesser Caucasus. Two groups of paleointensities averages have been obtained: (1) A combination of MSP-DSC results (from the present study) and Thellier-type under strict RCRIT criteria (from a previous study carried out by Sánchez-Moreno et al., 2020)

and, (2) the same MSP-DSC results and the Thellier-type determinations re-interpreted with less strict criteria TTP.

Absolute intensity determinations with the multispecimen technique were performed on 12 samples with both the original method (MSP-DB, Biggin & Poidras, 2006; Dekkers & Böhnel, 2006) and the extended protocol with corrections (Fabian & Leonhardt, 2010). In general, an overestimation of paleointensity results can be observed with the MSP-DB protocol with respect to MSP-DSC results. Therefore, MSP-DSC paleointensities have been chosen to perform averages with Thellier-type results. Eight MSP-DSC determinations from eight flows passed the proposed quality criteria. Each of the latter have been obtained by applying different values of the α parameter, which optimizes the Q_{DSC} ratios linear fit. It has been observed that the value $\alpha = 0.2$ has been the optimal for the MSP results independently of the thermomagnetic behavior and the hysteresis parameters in the specimens.

Combination of paleointensity results from Thellier-Thellier and IZZI determinations under TTP criteria and MSP-DSC experiments have been obtained in 11 lava flow. Four paleointensities belong to quality level 1 (MSP-DSC and TT/IZZI) and seven to quality 2 (TT an IZZI). The flow-average paleointensies obtained this way range from 12.5 to 24.6 μT in the lower reverse-polarity part of the sequence and the upper normal-polarity section provides higher values between 37.2 and 44.3 μT.

When we perform a similar analysis, combining the MSP-DSC results from the present study with Thellier-type results obtained under RCRIT criteria (Sánchez-Moreno et al., 2020), a single result of 36.9 μT (quality 1) is obtained in the normal polarity section. In the reverse polarity section, 3 results ranging from 19.2 to 24.1 μT (quality 1 and 2) could be determined. All of them show values similar to those obtained with the looser TTP criteria.

In addition, the other four results from a single Thellier-type (TT or IZZI) method under RCRIT criteria, presented in Sánchez-Moreno et al. (2020), have been classified as Category 3 (AP11, AP16, AP19, and AP20 in Table 5), because the filtering involved in applying this type of criteria restricts the results to data with a high quality, so that their reliability cannot be rejected. However, when the data come from different methods, such as in the other four cases (mostly where MSP-DSC is included), an increase of reliability is obtained.

With both approaches, the reverse polarity lower part yielded relatively low-paleointensity values, characteristic of pre-reversal stages (Laj & Channell, 2007). The relatively high paleointensity values recorded in the upper part of normal polarity may reflect the intensity recovery after a complete reversal.

The paleointensity values obtained in the previous work (Sánchez-Moreno et al., 2020) with Thelier-type methods under strict criteria are similar to those obtained in this study under a multi-method approach, whether we apply strict or more flexible criteria to the Thellier-type determinations, and combine both with MSP-DSC. The use of different methods is a quality criterion that must be presented in the paleointensity data to demonstrate enhanced reliability. The results obtained in this study allow us to conclude that it is not necessary to apply strict criteria, which may reject valid data subject to experimental noise, if a multi-method approach is used.

A detailed analysis of magnetic properties together with the analysis of the MSP and Thellier-type experiments, suggests that the thermomagnetic behavior and domain state can vary widely between adjacent specimens in this type of lava flows. This leads to different results depending on the type of paleointensity determination. Therefore, special care must be taken when applying the selection criteria and calculating the average paleointensity per lava flow.

Yet, no generalized agreement may be reached about the quality criteria used in MSP paleointensity determinations and their threshold values. In the present study we decided to use CI_{95} (95% confidence interval, see Multispecimen Paleointensity software online version http://ambre.gm.univ-montp2.fr/camps/MSP_DSC) over ΔB (ΔH in Fabian & Leonhardt, 2010) as a measure for the final uncertainty of the paleointensity determination. CI_{95} depends on the proximity and number of B_{lab} steps close to the final paleointensity obtained, so it evaluates a more instrumental character. ΔB evaluates domain state correction and alterations, which are already evaluated by ε_{alt}.

Data Availability Statement

Datasets for this research are available in these in-text data citation references: Sánchez-Moreno, E. M (2020). Thellier and multispecimen paleointensities from Apnia Pliocene volcanic sequence [Data set]. Zenodo. http://doi.org/10.5281/zenodo.3673186

References

Adamia, S., Zakariadze, G., Chkhotua, T., Sadradze, N., Tsereteli, N., Chabukiani, A., & Gventsadze, A. (2011). Geology of the Caucasus: A review. *Turkish Journal of Earth Science*, *20*, 489–544. https://doi.org/10.3906/yer-1005-11

Avagyan, A., Sosson, M., Karakhanian, A., Philip, H., Rebai, S., Rolland, Y., et al. (2010). Recent tectonic stress evolution in the Lesser Caucasus and adjacent regions. *Geological Society, London, Special Publications*, *340*, 393–408. https://doi.org/10.1144/sp340.17

Biggin, A., & Poidras, T. (2006). First-order symmetry of weak-field partial thermoremanence in multi-domain ferromagnetic grains. 1. Experimental evidence and physical implications. *Earth and Planetary Science Letters*, *245*, 438–453. https://doi.org/10.1016/j.epsl.2006.02.035

Biggin, A. J., Badejo, S., Muxworthy, A. R., & Dekkers, M. J. (2013). The effect of cooling rate on the intensity of thermoremanent magnetization (TRM) acquired by assemblages of pseudo-single domain, multidomain and interacting single-domain grains. *Geophysical Journal International*, *193*, 1239–1249. https://doi.org/10.1093/gji/ggt078

Biggin, A. J., & Paterson, G. a. (2014). A new set of qualitative reliability criteria to aid inferences on paleomagnetic dipole moment variations through geological time. *Frontiers of Earth Science*, *2*, 1–9. https://doi.org/10.3389/feart.2014.00024

Biggin, A. J., Piispa, E. J., Pesonen, L. J., Holme, R., Paterson, G. A., Veikkolainen, T., & Tauxe, L. (2015). Paleomagnetic field intensity variations suggest Mesoproterozoic inner-core nucleation. *Nature*, *526*, 245–248. https://doi.org/10.1038/nature15523

Bol'shakov, A. S., & Shcherbakova, V. (1979). A thermomagnetic criterion for determining the domain structure of ferrimagnetics. *Izv. Akad. Nauk. SSSR*, *15*, 111–117.

Calvo-Rathert, M., Bógalo, M. F., Gogichaishvili, A., Sologashvili, J., & Vashakidze, G. (2013). New paleomagnetic and paleointensity data from Pliocene lava flows from the Lesser Caucasus. *Journal of Asian Earth Sciences*, *73*, 347–361. https://doi.org/10.1016/j.jseaes.2013.04.039

Calvo-Rathert, M. C., Bógalo, M. F., Morales, J., Goguitchaichvili, A., Lebedev, V. A., Vashakidze, G., et al. (2020). An integrated paleomagnetic, multimethod-paleointensity and radiometric study on Cretaceous and Paleogene lavas from the Lesser Caucasus: Geomagnetic and tectonic implications. *Journal of Geophysical Research: Solid Earth*, *53*, 1689–1699. https://doi.org/10.1029/2020JB020019

Calvo-Rathert, M. C., Morales-Contreras, J., Carrancho, Á., & Goguitchaichvili, A. (2016). A comparison of Thellier-type and multispecimen paleointensity determinations on Pleistocene and historical lava flows from Lanzarote (Canary Islands, Spain). *Geochemistry, Geophysics, Geosystems*, *17*, 3638–3654. https://doi.org/10.1002/2016GC006396

Carvallo, C., Camps, P., Sager, W. W., & Poidras, T. (2017). Palaeointensity determinations and magnetic properties on Eocene rocks from Izu-Bonin-Mariana forearc (IODP Exp. 352). *Geophysical Journal International*, *210*, 1993–2009. https://doi.org/10.1093/gji/ggx208

Cromwell, G., Tauxe, L., Staudigel, H., & Ron, H. (2015). Paleointensity estimates from historic and modern Hawaiian lava flows using glassy basalt as a primary source material. *Physics of the Earth and Planetary Interiors*, *241*, 44–56. https://doi.org/10.1016/j.pepi.2014.12.007

Day, R., Fuller, M., & Schmidt, V. A. (1977). Hysteresis properties of titanomagnetites: Grain-size and compositional dependence. *Physics of the Earth and Planetary Interiors*, *13*, 260–267. https://doi.org/10.1016/0031-9201(77)90108-X

de Groot, L. V., Béguin, A., Kosters, M. E., van Rijsingen, E. M., Struijk, E. L. M., Biggin, A. J., et al. (2015). High paleointensities for the Canary Islands constrain the Levant geomagnetic high. *Earth and Planetary Science Letters*, *419*, 154–167. https://doi.org/10.1016/j.epsl.2015.03.020

de Groot, L. V., Biggin, A. J., Dekkers, M. J., Langereis, C. G., & Herrero-Bervera, E. (2013). Rapid regional perturbations to the recent global geomagnetic decay revealed by a new hawaiian record. *Nature Communications*, *4*, 1–7. https://doi.org/10.1038/ncomms3727

de Groot, L. V., Pimentel, A., & Di Chiara, A. (2016). The multimethod palaeointensity approach applied to volcanics from Terceira: Full-vector geomagnetic data for the past 50 kyr. *Geophysical Journal International*, *206*, 590–604. https://doi.org/10.1093/gji/ggw095

Dekkers, M. J., & Böhnel, H. N. (2006). Reliable absolute palaeointensities independent of magnetic domain state. *Earth and Planetary Science Letters*, *248*, 507–516. https://doi.org/10.1016/j.epsl.2006.05.040

Dunlop, D. J. (2002). Theory and application of the Day plot (Mrs /Ms versus Hcr/Hc) 2. Application to data for rocks, sediments, and soils. *Journal of Geophysical Research*, *107*, 2057. https://doi.org/10.1029/2001JB000487

Dunlop, D. J. (2011). Physical basis of the Thellier-Thellier and related paleointensity methods. *Physics of the Earth and Planetary Interiors*, *187*, 118–138. https://doi.org/10.1016/j.pepi.2011.03.006

Dunlop, D. J., & Özdemir, Ö. (2000). Effect of grain size and domain state on thermal demagnetization tails. *Geophysical Research Letters*, *27*(9), 1311–1314. https://doi.org/10.1029/1999GL008461

Dunlop, D. J., & Xu, S. (1994). Theory of partial thermoremanent magnetization in multidomain grains: 1. Repeated identical barriers to wall motion (single microcoercivity). *Journal of Geophysical Research: Solid Earth*, *99*, 9005–9023. https://doi.org/10.1029/93JB02566

Fabian, K., & Leonhardt, R. (2007). Theoretical analysis and experimental tests of multiple specimen absolute paleointensity determination techniques. *Geophysical Research Abstracts*, *9*, 04510.

Fabian, K., & Leonhardt, R. (2010). Multiple-specimen absolute paleointensity determination: An optimal protocol including pTRM normalization, domain-state correction, and alteration test. *Earth and Planetary Science Letters*, *297*, 84–94. https://doi.org/10.1016/j.epsl.2010.06.006

Fanjat, G. (2012). *Les fluctuations du champ magnétique terrestre : Des variations séculaires récentes aux renversements*. PhD. Géophysique, Universié de Montpellier, (p. 768). Retrieved from https://tel.archives-ouvertes.fr/tel-00719380/PDF/thesefanjat2012.pdf

Goguitchaichvili, A.T., Prévot, M., & Camps, P. (1999). No evidence for strong fields during the R3 – N3 Icelandic geomagnetic reversal. *Earth and Planetary Science Letters*, *167*, 15–34. https://doi.org/10.1016/S0012-821X(99)00010-2

Haggerty, S. E. (1991). Oxide Textures: A Mini-Atlas. In D. H. Lindsley (Ed.), Oxide minerals: Petrologic and magnetic significance, Rev. Mineral. (Vol. 25, pp. 129–137). Washington, D. C. Mineral. Society of America.

Heller, R., Merrill, R.T., & McFadden, P.L. (2002). The variation of intensity of earth's magnetic field with time. *Physics of the Earth and Planetary Interiors*, *131*, 237–249. https://doi.org/10.1016/S0031-9201(02)00038-9

Herrero-Bervera, E., & Valet, J.-P. (1999). Paleosecular variation during sequential geomagnetic reversals from Hawaii. *Earth and Planetary Science Letters*, *171*, 139–148. https://doi.org/10.1016/S0012-821X(99)00145-4

Juarez, M. T., & Tauxe, L. (2000). The intensity of the time-averaged geomagnetic field: The last 5 Myr. *Earth and Planetary Science Letters*, *175*, 169–180. https://doi.org/10.1016/S0012-821X(99)00306-4

Juárez, M. T., Tauxe, L., Gee, J. S., & Pick, T. (1998). The intensity of the Earth's magnetic field over the past 160 million years. *Nature*, *394*, 878–881. https://doi.org/10.1038/29746

Laj, C., & Channell, J. E. T. (2007). 5.10 - Geomagnetic Excursions. In G. Schubert (Ed.), *Treatise on geophysics*. (Vol. 5, pp. 373–416). Elsevier. https://doi.org/10.1016/B978-044452748-6.00095-X

Lawrence, K. P., Tauxe, L., Staudigel, H., Constable, C. G., Koppers, A., McIntosh, W., & Johnson, C. L. (2009). Paleomagnetic field properties at high southern latitude. *Geochemistry, Geophysics, Geosystems*, *10*. https://doi.org/10.1029/2008GC002072

Lebedev, V. A., Bubnov, S. N., Dudauri, O. Z., & Vashakidze, G. T. (2008). Geochronology of Pliocene volcanism in the Dzhavakheti Highland (the Lesser Caucasus). Part 1: Western part of the Dzhavakheti Highland. *Stratigraphy and Geological Correlation*, *16*, 204–224. https://doi.org/10.1134/S0869593808020081

Leonhardt, R., Heunemann, C., & Krasa, D. (2004). Analyzing absolute paleointensity determinations: Acceptance criteria and the software ThellierTool4.0. *Geochemistry, Geophysics, Geosystems*, *5*(12), 1–11. https://doi.org/10.1029/2004GC000807

Maisuradze, G. M., & Kuloshvili, S. I. (1999). Some geological problems of Late Volcanism in the Dzhavakheti Upland. *Tr. GIN AN Gruz. Nov. Ser.*, *114*, 220–228.

McFadden, P. L., & McElhinny, M. W. (1982). Variations in the geomagnetic dipole 2: Statistical analysis of VDMs for the past 5 million years. *Journal of Geomagnetism and Geoelectricity*, *34*, 163–189. https://doi.org/10.5636/jgg.34.163

Michalk, D. M., Biggin, A. J., Knudsen, M. F., Böhnel, H. N., Nowaczyk, N. R., Ownby, S., & López-Martínez, M. (2010). Application of the multispecimen palaeointensity method to Pleistocene lava flows from the Trans-Mexican Volcanic Belt. *Physics of the Earth and Planetary Interiors*, *179*, 139–156. https://doi.org/10.1016/j.pepi.2010.01.005

Michalk, D. M., Muxworthy, A. R., Böhnel, H. N., Maclennan, J., Nowaczyk, N., Harald, N. B., et al. (2008). Evaluation of the multispecimen parallel differential pTRM method: A test on historical lavas from Iceland and Mexico. *Geophysical Journal International*, *173*, 409–420. https://doi.org/10.1111/j.1365-246X.2008.03740.x

Monster, M. W. L., de Groot, L. V., Biggin, A. J., & Dekkers, M. J. (2015). The performance of various palaeointensity techniques as a function of rock magnetic behavior - A case study for La Palma. *Physics of the Earth and Planetary Interiors*, *242*, 36–49. https://doi.org/10.1016/j.pepi.2015.03.004

Monster, M. W. L., de Groot, L. V., & Dekkers, M. J. (2015). MSP-Tool: A VBA-Based software tool for the analysis of multispecimen paleointensity data. *Frontiers of Earth Science*, *3*, 1–9. https://doi.org/10.3389/feart.2015.00086

Monster, M. W. L., Langemeijer, J., Wiarda, L. R., Dekkers, M. J., Biggin, A. J., Hurst, E. A., & Groot, L. V. d. (2018). Full-vector geomagnetic field records from the East Eifel, Germany. *Physics of the Earth and Planetary Interiors*, *274*, 148–157. https://doi.org/10.1016/j.pepi.2017.11.009

Paterson, G. A. (2011). A simple test for the presence of multidomain behavior during paleointensity experiments. *Journal of Geophysical Research: Solid Earth*, *116*(10), 1–12. https://doi.org/10.1029/2011JB008369

Paterson, G. A. (2013). The effects of anisotropic and non-linear thermoremanent magnetizations on Thellier-type paleointensity data. *Geophysical Journal International*, *193*, 694–710. https://doi.org/10.1093/gji/ggt033

Paterson, G. A., Biggin, A. J., Hodgson, E., & Hill, M. J. (2015). Thellier-type paleointensity data from multidomain specimens. *Physics of the Earth and Planetary Interiors*, *245*, 117–133. https://doi.org/10.1016/j.pepi.2015.06.003

Paterson, G. A., Tauxe, L., Biggin, A. J., Shaar, R., & Jonestrask, L. C. (2014a). On improving the selection of Thellier-type paleointensity data. *Geochemistry, Geophysics, Geosystems*, *15*, 1180–1192. https://doi.org/10.1002/2013GC005135

Paterson, G. A., Tauxe, L., Biggin, A. J., Shaar, R., & Jonestrask, L. C. (2014b). *Standard Paleointensity Definitions v1.1 0–43*. Retrieved from https://earthref.org/PmagPy/SPD/DL/SPD_v1.2.0.pdf

Prévot, M., Mankinen, E. A., Coe, R. S., & Grommé, C. S. (1985). The Steens Mountain (Oregon) geomagnetic polarity transition: 2. Field intensity variations and discussion of reversal models. *Journal of Geophysical Research*, *90*, 10417–10448. https://doi.org/10.1029/JB090iB12p10417

Prévot, M., Mankinen, E. A., Grommé, C. S., & Coe, R. S. (1985). How the geomagnetic field vector reverses polarity. *Nature*, *316*, 230–234. https://doi.org/10.1038/316230a0

Riisager, J., Perrin, M., Riisager, P., & Ruffet, G. (2000). Paleomagnetism, paleointensity and geochronology of Miocene basalts and baked sediments from Velay Oriental, French Massif Central. *Journal of Geophysical Research*, *105*, 883–896. https://doi.org/10.1029/1999JB900337

Roberts, A. P., Tauxe, L., Heslop, D., Zhao, X., & Jiang, Z. (2018). A critical appraisal of the "Day" diagram. *Journal of Geophysical Research: Solid Earth*, *123*, 2618–2644. https://doi.org/10.1002/2017JB015247

Sánchez-Moreno, E. M., Calvo-Rathert, M., Goguitchaichvili, A., Tauxe, L., Vashakidze, G. T., & Lebedev, V. A. (2020). Weak palaeointensity results over a Pliocene volcanic sequence from Lesser Caucasus (Georgia): Transitional record or time averaged field? *Geophysical Journal International*, *220*(3), 1604–1618. https://doi.org/10.1093/gji/ggz533

Sánchez-Moreno, E. M., Calvo-Rathert, M., Goguitchaichvili, A., Vashakidze, G. T., & Lebedev, V. A. (2018). Evidence of unusual geomagnetic regimes recorded in Plio-Pleistocene Volcanic Sequences from the Lesser Caucasus (Southern Georgia). *Geochemistry, Geophysics, Geosystems*, *19*, 1–18. https://doi.org/10.1029/2017GC007358

Selkin, P. A., & Tauxe, L. (2000). Long-term variations in palaeointensity. *Philosophical Transactions of the Royal Society of London, Series A: Mathematical, Physical and Engineering Sciences*, *358*(1768), 1065–1088. https://doi.org/10.1098/rsta.2000.0574

Selkinx, P. A., Gee, J. S., & Tauxe, L. (2007). Nonlinear thermoremanence acquisition and implications for paleointensity data. *Earth and Planetary Science Letters*, *256*, 81–89. https://doi.org/10.1016/j.epsl.2007.01.017

Tanaka, H., Athanassopoulos, J. D. E., Dunn, J. R., & Fuller, M. (1995). Paleointensity determinations with measurements at high-temperature. *Journal of Geomagnetism and Geoelectricity*, *47*, 103–113. https://doi.org/10.5636/jgg.47.103

Tauxe, L. (2006). Long-term trends in paleointensity: The contribution of DSDP/ODP submarine basaltic glass collections. *Physics of the Earth and Planetary Interiors*, *156*, 223–241. https://doi.org/10.1016/j.pepi.2005.03.022

Tauxe, L., Gee, J. S., Steiner, M. B., & Staudigel, H. (2013). Paleointensity results from the Jurassic: New constraints from submarine basaltic glasses of ODP Site 801C. *Geochemistry, Geophysics, Geosystems*, *14*, 4718–4733. https://doi.org/10.1002/ggge.20282

Tauxe, L., Shaar, R., Jonestrask, L., Swanson-Hysell, N. L., Minnett, R., Koppers, A. A. P., et al. (2016). PmagPy: Software package for paleomagnetic data analysis and a bridge to the Magnetics Information Consortium (MagIC) Database. *Geochemistry, Geophysics, Geosystems*, *17*, 2450–2463. https://doi.org/10.1002/2016GC006307

Tema, E., Ferrara, E., Camps, P., Conati Barbaro, C., Spatafora, S., Carvallo, C., et al. (2016). The Earth's magnetic field in Italy during the Neolithic period: New data from the Early Neolithic site of Portonovo (Marche, Italy). *Earth and Planetary Science Letters*, *448*, 49–61. https://doi.org/10.1016/j.epsl.2016.05.003

Thellier, E., & Thellier, O. (1959). Sur líntensité du champ magnétique terrestre dans le passé historique et géologique. *Annales Geophysicae*, *15*, 285–376.

Valet, J.-P., & Fournier, A. (2016). Deciphering records of geomagnetic reversals. *Reviews of Geophysics*, *54*, 410–446. https://doi.org/10.1002/2015RG000506

Valet, J. P., Meynadier, L., & Guyodo, Y. (2005). Geomagnetic dipole strength and reversal rate over the past two million years. *Nature*, *435*, 802–805. https://doi.org/10.1038/nature03674

Wang, H., Kent, D. V., & Rochette, P. (2015). Weaker axially dipolar time-averaged paleomagnetic field based on multidomain-corrected paleointensities from Galapagos lavas. *Proceedings of the National Academy of Sciences*, *112*, 15036–15041. https://doi.org/10.1073/pnas.1505450112

Yu, Y., Tauxe, L., & Genevey, A. (2004). Toward an optimal geomagnetic field intensity determination technique. *Geochemistry, Geophysics, Geosystems*, *5*. https://doi.org/10.1029/2003GC000630